Dating Ice Cores with the 36Cl/10Be Ratio

Kappelt, Niklas

2025

Document Version:
Publisher's PDF, also known as Version of record

LUNDQUA THESIS 99

Dating Ice Cores with the $^{36}Cl/^{10}Be$ Ratio

NIKLAS KAPPELT
QUATERNARY SCIENCES | DEPARTMENT OF GEOLOGY | LUND UNIVERSITY 2025

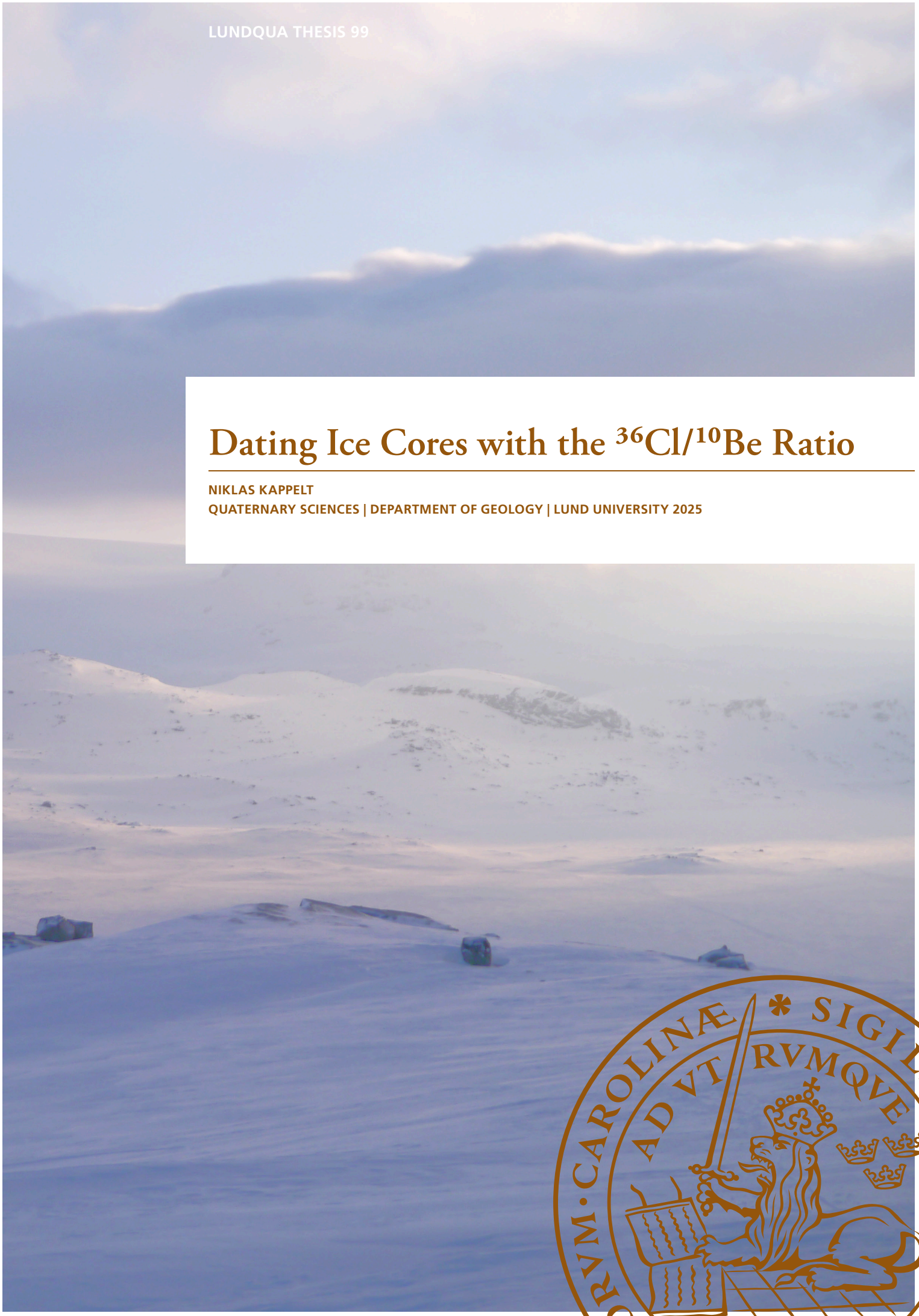

LUNDQUA THESIS 99

Dating Ice Cores with the $^{36}Cl/^{10}Be$ Ratio

Niklas Kappelt

LUND
UNIVERSITY

Quaternary Sciences
Department of Geology

DOCTORAL DISSERTATION

by due permission of the Faculty of Science, Lund University, Sweden.
To be defended at the Department of Geology, Lund University, on the 17th of October 2025 at 13:00.

Faculty opponent

Professor Robert Bingham
University of Edinburgh, Scotland

Published by:
Department of Geology
Faculty of Science
Lund University
Lund 2025

ISBN: 978-91-87847-92-9 (print)
ISBN: 978-91-87847-93-6 (pdf)
ISSN: 0281-3033

Printed in Sweden by Media-Tryck, Lund University,
Lund 2025

Organisation
Lund University
Department of Geology
Sölvegatan 12
223 62 Lund
Sweden

Document name
Doctoral Dissertation

Date of issue
17.10.2025

Author
Niklas Kappelt

Sponsoring organisation
European Commission

Title
Dating Ice Cores with the $^{36}Cl/^{10}Be$ Ratio

Abstract

Ice cores are unique archives of paleo-climate information and require accurate dating for its interpretation. Continuous chronologies are usually based on time markers, stratigraphic matching, and orbital tuning, but often end several meters above bedrock, because extreme thinning and sometimes disturbances in the stratigraphy complicate the identification of climate signals and their alignment with other records in the deepest ice. Independent age estimates can be obtained with the radioactive decay of ^{36}Cl and ^{10}Be, two radionuclides, which are produced in atmospheric spallation reactions initiated by galactic cosmic rays. Since the flux of these rays is modulated by the magnetic fields of the Sun and the Earth, individual concentrations vary over time, but their ratio is theoretically independent of production variations and decays with a half-life of 384 thousand years.

In this thesis, the application of the $^{36}Cl/^{10}Be$ ratio as a dating tool was tested and developed with a focus on three key challenges. Due to the different chemical properties of ^{36}Cl and ^{10}Be, they are transported and deposited differently, so their concentrations as well as the $^{36}Cl/^{10}Be$ ratio exhibit a variability in ice, which determines most of the age estimate uncertainty, as the initial $^{36}Cl/^{10}Be$ ratio at the time of deposition can only be estimated. A deuterium-based climate correction was applied to radionuclide data from a drill site in coastal West Antarctica and a remote drill site in East Antarctica, reducing uncertainties significantly. A second challenge for the dating method is a loss of volatile $H^{36}Cl$ at low accumulation sites. However, we were able to show that this mostly affects ice from interglacial periods, not from glacial periods, and that the loss is captured by the general trend of higher $^{36}Cl/^{10}Be$ ratios in colder times, which means the initially present ^{36}Cl can be estimated. A decrease of ^{10}Be concentrations with age faster than possible through radioactive decay alone poses a third challenge. It is likely related to an increasing association of ^{10}Be with dust over time. Testing various variations of the standard sample procedure, we found that passing samples through ion exchange columns resulted in systematically lower ^{10}Be concentrations compared to directly precipitated samples, suggesting they prevented the quantitative detection of ^{10}Be in previous analyses.

The improved dating method was tested on ice from the 800 thousand-year-old EPICA Dome C ice core and was in agreement with the established age scale. It was also used to estimate the age of the deepest part of the Skytrain ice core in West Antarctica and revealed that the ice in this location has been around for at least 500 thousand years, whereas it was previously hypothesised that the West Antarctic Ice Sheet melted in the last interglacial period. As several other bottommost ice core sections have not been dated so far, the method will be able to extend other age scales and help understand the history of the Earth's ice sheets better in the future.

ISSN and key title
0281-3033 LUNDQUA THESIS

Key words
Cosmogenic radionuclides, ice cores, dating, ^{36}Cl, ^{10}Be

ISBN (print)
978-91-87847-92-9

Language
English

ISBN (pdf)
978-91-87847-93-6

Number of pages
96

Signature

03.09.2025
Date

Acknowledgements

I would like to thank my supervisor Raimund, for introducing me to the interesting field of radionuclides, always making time for a meeting and creating a stimulating workspace for our research group. You struck a great balance between guidance and freedom in my research, while providing support whenever I needed it. Having tasted at least three different cakes at each of your birthday parties I know you could have been a professional baker, too, but I think you're doing even better as a professor. I want to thank Eric, my second supervisor, for happily discussing any idea I had and for navigating me through the labs and storage rooms in Cambridge all the way to the cold room to cut the ice from the Skytrain core with me.

Thank you Marie, for wonderfully organising all of the DEEPICE meetings and activities, and thank you to all DEEPICE students, I thoroughly enjoyed our training schools, expeditions, and conference meetups. It was inspiring for me to update each other about our research and it has been incredibly fun to travel, swim, barbecue, dance, and hike together.

I would also like to thank all the great people from the Geology department for the pleasant work atmosphere, hundreds of fikas, and fun after-work gatherings. Especially Qin for being a great office mate, all PhD students for the talks during lunch and the evenings we spend in Lund, and Andreas for stimulating conversations, making me laugh, and always offering to get the next round.

I would like to thank my parents, Heide and Klaus, for supporting me throughout my studies. It's been ten years since I finished school and moved out and I like to think that I became independent sometime halfway between returning home to do laundry and moving to another country, but knowing that I can always rely on you gave me a sense of security which let me take on and enjoy this Scandinavian adventure with excitement and curiosity.

I also want to thank my lovely partner, Elena, for encouraging me, bringing life to the home office, and making sure that every milestone along the way was celebrated. You are an inspiration and I will always be thankful for your support, your love, and the happiness you bring me.

Contents

Popular summary

The Greenland and Antarctic ice sheets contain a vast amount of information about the Earth's past climate. Snow has been accumulating in these regions for hundreds of thousands of years, trapping atmospheric air, which is stored as bubbles in the ice. Researchers access this information by drilling into the ice, extracting a core and analysing the atmospheric gas concentrations, the chemical composition, and other parameters. Age scales are developed to describe the relationship between the depth of a core and its age, which is essential to know for the interpretation of climate data. They use different sources of information, such as counted annual layers, synchronised climate data from different records, and absolute age markers, for example volcanic eruptions, which can be identified in the stratigraphy, all while considering snow accumulation, ice densification and ice flow.

However, these traditional methods have their limitations, as they require the reliable identification and synchronisation of time markers with other archives. Both become increasingly difficult to achieve with depth, as the temporal resolution decreases, often leaving several meters at the bottom of an ice core undated. Absolute age estimates can help verify and extend existing chronologies in deep ice. The $^{36}Cl/^{10}Be$ ratio has the potential for such estimates. ^{36}Cl and ^{10}Be are radionuclides, which are created in atmospheric reactions initiated by radiation coming from space. The radiation is variable, so the production rate of individual radionuclides varies over time, but their ratio is theoretically constant. Both are deposited on the ice sheets and their concentrations can be measured in ice cores. Since they are unstable and radioactively decay over time, lower concentrations are found in older ice, which can be used to estimate its age. The half-life of the ratio is 384 thousand years, which means ice of this age will have a $^{36}Cl/^{10}Be$ ratio half as high as the ratio in present-day snow.

In reality, the application is slightly more complicated. The $^{36}Cl/^{10}Be$ ratio in ice varies with the climate, as ^{36}Cl and ^{10}Be are different elements, which are transported and deposited differently. In our research, we were able to estimate the influence of the climate and apply a correction, which significantly improved the precision of age estimates. A second issue is the loss of ^{36}Cl at low accumulation sites, where gaseous $H^{36}Cl$ can be formed and escape the snow before it turns into ice. We were able to show that this mainly affects ice from warm, interglacial periods, while ^{36}Cl in ice from cold, glacial periods is preserved. Additionally, it was possible to estimate the amount which was lost and calculate back the ^{36}Cl concentrations of the initially deposited snow. A third challenge was posed by unexpected behaviour of ^{10}Be in deep ice. Concentrations were lower than expected and decreased faster with depth and age than possible through radioactive decay alone, which can distort age estimates. Our research suggests that an extraction step in the standard sample preparation procedure may lead to a loss of ^{10}Be, preventing a quantitative extraction in deep ice. The extraction step can be skipped if the sample size is small, but the mechanism should be researched further to ensure a quantitative extraction in future measurements.

It has been suggested that the West Antarctic Ice Sheet melted in the last interglacial period about 120 thousand years ago, as it was warmer and the sea-level was 6 to 9 meters higher than today. An ice core drilled in West Antarctica was previously dated to an age of 126 thousand years old, showing that the ice sheet did not disappear. The bottommost 24 meters of ice could not be dated with traditional methods, but with the help of the $^{36}Cl/^{10}Be$ ratio we were able to show that the ice sheet not only survived the last interglacial period, but has been present for at least 500 thousand years. With the improvements achieved for the dating method, other basal ice sections from Greenland and Antarctica can be dated in the future as well.

Abbreviations

ACR	Antarctic Cold Reversal
ADD	Antarctic Digital Database
AICC	Antarctic Ice Core Chronology
ATTA	Atom Trap Trace Analysis
BEOI	Beyond EPICA Oldest Ice
BP	Before Present
EDC	EPICA Dome C
EDML	EPICA Dronning Maud Land
EPICA	European Project for Ice Coring in Antarctica
GCR	Galactic Cosmic Ray
GRIP	Greenland Ice Core Project
IEC	Ion Exchange Column
LASM	Large Area Scanning Microscope
LDC	Little Dome C
LGM	Last Glacial Maximum
LIS	Local Interstellar Spectrum
WAIS	West Antarctic Ice Sheet

List of publications

This thesis is based on the following publications, referred to by their Roman numerals:

Paper I

Ice core dating with the $^{36}Cl/^{10}Be$ ratio

Niklas Kappelt, Raimund Muscheler, Mélanie Baroni, Juerg Beer, Marcus Christl, Christof Vockenhuber, Edouard Bard, ASTER Team, and Eric Wolff

Quaternary Science Reviews, 355: 109254, May 2025

https://doi.org/10.1016/j.quascirev.2025.109254

Available in open access.

Paper II

500-thousand-year-old basal ice at Skytrain Ice Rise, West Antarctica, estimated with the $^{36}Cl/^{10}Be$ ratio

Niklas Kappelt, Eric Wolff, Marcus Christl, Christof Vockenhuber, Philipp Gautschi, and Raimund Muscheler

Climate of the Past, 2025

https://doi.org/10.5194/egusphere-2025-1780

In press, will be available in open access.

Paper III

Post-depositional processes of ^{10}Be in deep ice

Niklas Kappelt, Piers Larkman, Pascal Bohleber, Florian Adolphi, Marcus Christl, Christof Vockenhuber, Philipp Gautschi, Eric Wolff, and Raimund Muscheler

Manuscript

1 Motivation

Ice cores are unique paleo-climate archives, as they contain the only direct record of the past atmosphere, as well as a plethora of isotopes and impurities which can be used as climate proxies. The compiled carbon dioxide record over the last 800 kyr, for example, demonstrates the slow natural variability of atmospheric CO_2 concentrations between 190 and 280 ppm, which is strongly contrasted by the sharp increase over the last few decades, reaching 427 ppm in 2025 (10).

Current research is aimed at retrieving a continuous ice core as old as 1,500 kyr to investigate the mid-Pleistocene transition, which lasted from about 1,200 until 700 kyr ago and describes a change in the periodicity of glacial-interglacial cycles from 41 to 100 kyr (14). A preliminary analysis of the core suggests 1,200 kyr old ice at a depth of 2,480 m, while bedrock was reached at a depth of 2,800 m in 2024 (15). Similar to other ice cores from Greenland and Antarctica, the bottommost section is challenging to date, since the temporal resolution decreases as the ice is stretched thin from the enormous weight of the ice sheet resting above it (89, 100). Additionally, disturbances in the stratigraphy are possible, complicating the identification of time markers used to constrain the age scale or to synchronise it with existing chronologies (24, 33, 37, 60). For the interpretation of any proxy data, however, a reliable age scale is crucial.

Cosmogenic radionuclides, such as ^{36}Cl and ^{10}Be, are produced in the atmosphere and deposited on the polar ice sheets, where they decay over time, so they have the potential to provide absolute age estimates, independent of existing chronologies and stratigraphic disturbances. The ^{36}Cl/^{10}Be ratio was first suggested to be used as a dating tool in the 1980s by Nishiizumi et al. in Antarctica and Elmore et al. in Greenland (30, 65). The aim of this thesis was to test the dating method on ice of known age, improve it, and apply it to ice of unknown age from Antarctica. Three challenges, outlined in sections 2.2, 2.3, and 2.4, respectively, were identified and partly overcome: the variability of the deposition flux, which determines most of the age estimate uncertainty, the reversible deposition of ^{36}Cl in firn, which can lead to poor signal preservation, and the mobility of ^{10}Be in deep ice, which can alter the original signal.

2 Background

2.1 Radionuclide production

Radionuclides are produced by nuclear reactions in the atmosphere, initiated by galactic cosmic rays (GCRs). These rays originate from supernovae in the Milky Way and consist mostly of protons, alpha particles, heavier nuclei, and electrons, which reach our solar system with an essentially isotropic intensity distribution known as the local interstellar spectrum (LIS). In the heliosphere, the energy spectrum is modulated, because the movement of plasma inside the Sun generates a magnetic field which is carried out into space by the solar wind, deflecting electrically charged GCRs (11). An accurate description of all interactions requires complex equations, which are impractical to use, but the differential energy spectrum near Earth $J(T, \Phi)$ resulting from the overall modulation of the LIS by the solar magnetic field in the Heliosphere can be quantified with the empirical solar modulation function Φ in MeV in the force field approximation as

$$J(T, \Phi) = J_{\mathrm{LIS}}(T + \Phi)\frac{T^2 - E_0^2}{(T + \Phi)^2 - E_0^2}, \tag{1}$$

where J_{LIS} is the differential energy cosmic ray flux outside the Heliosphere and T and E_0 are the respective total and rest mass energy of a cosmic ray particle (36). Figure 1 shows the LIS model of Herbst et al. (43) for protons and the effect that different values of Φ have on the spectrum. Φ is GCR component specific and calculated from the solar modulation potential φ in MV as $\Phi = Ze\varphi$, where Z is the atomic number and e is the elemental charge.

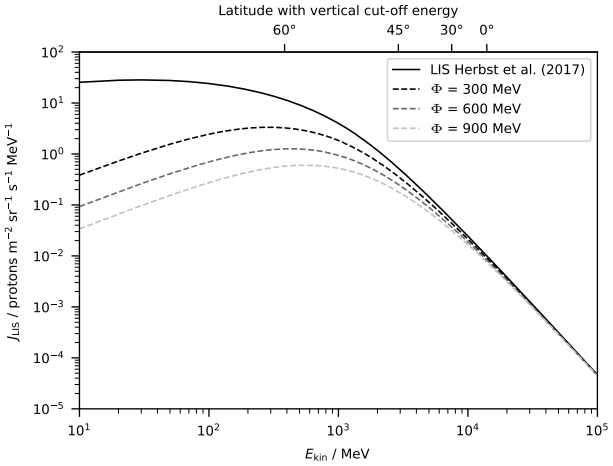

Figure 1: The local interstellar spectrum of protons after Herbst et al. (43), the effect of different values for the solar modulation function Φ and vertical cut-off energies of selected geomagnetic latitudes.

The geomagnetic field of the Earth constitutes a second stage of deflection for GCRs and creates a highly regional distribution of the flux reaching the atmosphere. For the discussion of radionuclide production, it is usually sufficient to consider the dipole component, whose field lines are perpendicular to vertically arriving cosmic rays at the equator, but parallel at the geomagnetic poles, leading to a strong latitude dependence of the GCR flux with higher values at the geomagnetic poles (11). The particle rigidity R is defined as the momentum to charge ratio and describes a particle's resistance to deflection by the geomagnetic field. It can be expressed as

$$R = \frac{A}{Z}\sqrt{(E_0 + E)^2 - E_0^2}, \tag{2}$$

where A and Z are the particle's atomic mass number and charge number, respectively, E_0 is its rest mass energy and E is its kinetic energy. For a magnetic dipole moment M, it is possible to calculate a latitude dependent geomagnetic cut-off rigidity $R_{\mathrm{c}}(\lambda)$, which is the minimum rigidity required for a particle to penetrate the geomagnetic field and reach the Earth. For vertically arriving cosmic rays, it can be calculated as

$$R_{\mathrm{c,v}}(\lambda) = \frac{14.9M}{M_0}\cos^4(\lambda), \tag{3}$$

where $M_0 = 7.8 \times 10^{22}\,\mathrm{A\,m^2}$ is the present-day dipole moment of the geomagnetic field (2). The relationship between rigidity R and energy per nucleon E described in Equation 2 was used to calculate examples for cut-off energies corresponding to specific latitudes in Figure 1. While all vertically arriving particles can penetrate the Earth at the geomagnetic poles, increasingly higher energies are needed towards the equator.

Once in the atmosphere, primary cosmic ray particles initiate a cascade of nuclear reactions. Alpha and heavier particles break up into their constituent nucleons upon first impact with an atmospheric nucleus and subsequent reactions occur with secondary protons and neutrons until the initial energy is dissipated. In this cascade of reactions, cosmogenic radionuclides can be produced by spallation reactions on heavier nuclei or through neutron capture. The production rate P of a radionuclide j at an atmospheric depth X, defined as the weight per area above a certain height in the atmosphere, is the sum over all reactions between secondary cosmic ray particles k (protons and neutrons) and target nuclei i (N_2, O_2, Ar, ...), integrated over the entire energy spectrum of the cosmic ray flux. It is given as

$$P_j(X) = \sum_i N_i \sum_k \int_0^\infty \sigma_{jik}(E_k) \cdot J_k(\phi, R_{\mathrm{c}}, E_k, X)\,\mathrm{d}E_k, \tag{4}$$

where N_i is the density of a target nucleus i in atoms g^{-1} and $\sigma_{jik}(E_k)$ is the cross section for a specific reaction between a target nucleus i and a cosmic ray particle component k to produce radionuclide j in cm^2. The central idea of this thesis is to date ice cores using the radionuclides ^{36}Cl, produced in reactions with argon, and ^{10}Be, generated through interactions with nitrogen and oxygen. Although reactions yielding ^{36}Cl exhibit considerably larger cross-sections, the vastly higher atmospheric abundances of nitrogen and oxygen compared to argon result in ^{10}Be production rates that exceed those of ^{36}Cl by about an order of magnitude.

Global radionuclide production rates are not constant, because the LIS, the solar magnetic field, and the geomagnetic field can change over time. Short-term variations are dominated by changes in the solar magnetic field, whose amplitude increases and decreases with a 11-year periodicity. With the present-day value for the geomagnetic field, the 9,400-year reconstruction of the solar modulation function by Steinhilber et al. (85) with a resolution of 22 years suggests a 13 % standard deviation from the mean for the ^{36}Cl and ^{10}Be production rates, caused by variations in the strength of the solar magnetic field. Over longer timescales, production rate changes are dominated by changes in the geomagnetic field. A reconstruction of it by Channell et al. (19) with a resolution of 1,000 years suggests a 26 % standard deviation from the mean over the last 1.5 million years. As our solar system rotates around the centre of the Milky Way, it passes in and out of its spiral arms, which presumably leads to higher and lower LIS intensities (18). However, this occurs on timescales of tens of millions of years, far longer than typical ice core ages. For the intent of dating ice, the LIS can, therefore, be regarded as constant.

While these influences on production rates make radionuclide records a powerful tool for reconstructions of geomagnetic and solar magnetic field strengths (9, 62, 63, 64, 93, 104) and chronology alignment through peak synchronisation (1, 22), they complicate radioactive decay dating by overlaying the decay signal with a changing production signal. As ^{36}Cl and ^{10}Be are affected in a similar way, however, their production rate ratio of 0.086 is theoretically independent of the varying magnetic field strengths, as shown in Figure 2. It has a half-life of 384 kyr, resulting from the half-lives of 301 kyr for ^{36}Cl and 1,387 kyr for ^{10}Be, respectively (20, 31, 52). A production related difference of 25 % between the ^{36}Cl concentrations in two samples could be misinterpreted as a decay signal, which would suggest an age difference of 150 kyr, while the ^{36}Cl/^{10}Be ratio would be unaffected by the production rate difference.

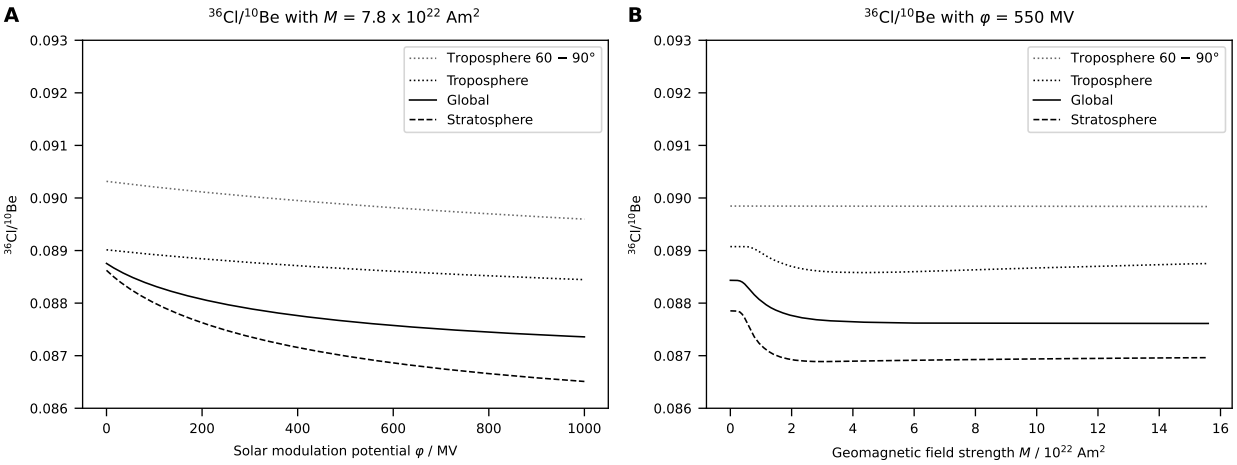

Figure 2: Influences of **A** solar modulation and **B** the geomagnetic field on the ^{36}Cl/^{10}Be production rate ratio in different atmospheric domains.

2.2 Transport and deposition

The number of available cosmic ray particles with sufficient energy to generate additional radionuclides decreases with atmospheric depth, resulting in approximately two thirds of radionuclide production occurring in the stratosphere and one third in the troposphere (38, 39, 70). For the stratosphere, a residence time of one to two years has been estimated for both, ^{36}Cl and ^{10}Be (40, 41, 72, 88), and their primary pathway into the troposphere is

the exchange of air masses across the tropopause at mid-latitudes, where also the highest deposition fluxes are observed globally. In other regions, the precipitation rate largely determines the deposition flux, as wet removal is more effective than dry deposition, resulting in a global distribution that does not directly reflect the latitude dependent production profile (32, 38, 105): the production is highest at the geomagnetic poles, but Greenland and Antarctica are amongst the regions with the lowest radionuclide deposition fluxes.

Once deposited, the ^{36}Cl/^{10}Be ratio R decays with

$$R = R_0 \cdot \mathrm{e}^{-kt}, \tag{5}$$

where R_0 is the initially deposited ratio, k is the decay constant given by $k = \frac{\ln(2)}{t_{1/2}}$ and R is the ratio after a time t in years. In a sample of unknown age, the time since deposition can be calculated as

$$t = -\frac{1}{k} \ln\left(R/R_0\right). \tag{6}$$

However, the initial ^{36}Cl/^{10}Be ratio at the time of deposition is usually unknown. Even though the ^{36}Cl/^{10}Be production rate ratio is constant in time, the measured ^{36}Cl/^{10}Be ratio in ice is not. It is site-specific, and varies significantly within a given record, as demonstrated in Table 1, which lists the mean ^{36}Cl/^{10}Be ratios measured in different, Antarctic and Greenland ice cores with their respective, relative standard deviations from the mean.

Table 1: Mean, decay-corrected ^{36}Cl/^{10}Be ratios in different ice cores (7, 47, 56, 94, 101).

Ice core	Time period	Mean ^{36}Cl/^{10}Be	σ_{relative}
Dome Fuji	7,440–7,362 yr BP	0.12	19 %
Dye3	527–40 yr BP	0.15	44 %
GRIP	307–102,000 yr BP	0.26	25 %
Milcent	761–129 yr BP	0.18	30 %

The initial ^{36}Cl/^{10}Be ratio of an undated sample can, therefore, neither be assumed to reflect the production rate ratio of 0.086 nor to be identical to a single measurement of the ratio in recent precipitation. However, it can be estimated with the mean, decay-corrected ^{36}Cl/^{10}Be ratio measured in ice of known age from the same site. The uncertainty of the mean value $\sigma(R_0)$ can be estimated with the one-σ standard deviation from the mean. It directly affects the uncertainty of the estimated age $\sigma(t)$ with

$$\sigma(t) = \frac{\mathrm{d}t}{\mathrm{d}R_0} \cdot \sigma(R_0) = \frac{1}{kR_0} \cdot \sigma(R_0), \tag{7}$$

showing that the absolute uncertainty of age estimates scales linearly with the relative uncertainty of the mean initial ratio, about 5.5 kyr per percentage point. It is, therefore, desirable to understand what causes the variability of the ^{36}Cl/^{10}Be ratio and whether there is a climatic influence that can be removed from the signal to reduce it and thereby lower the dating uncertainty.

The deposited ratio is a likely product of the different transport and deposition mechanisms of ^{36}Cl and ^{10}Be related to their physical and chemical properties: ^{36}Cl predominantly forms hydrogen chloride gas, while ^{10}Be attaches to aerosols (41, 42, 103, 105). As shown in Table 1, the mean ^{36}Cl/^{10}Be ratio is higher than the production rate ratio of 0.086 in all ice core records, which suggests a depletion of ^{10}Be in respect to ^{36}Cl in polar precipitation. A possible mechanism for this is the rainout (in-cloud) or washout (below-cloud) of ^{10}Be in air masses moving from mid-latitudes towards the poles (61, 67, 68). While ^{36}Cl is likely to be removed as well, the degree of depletion may be lower. Measurements in precipitation samples from Indiana in the United States and Switzerland showed an increase of the ^{36}Cl/^{10}Be ratio throughout the course of individual precipitation events,

supporting the hypothesis of a faster ^{10}Be removal (51, 56). While a preferential removal of ^{10}Be could increase the long-term mean ^{36}Cl/^{10}Be ratio, it would also have the potential to cause short-term variability, related to the amount of precipitation en-route. The modelled radionuclide deposition flux of a recent modelling study showed an increasing trend for the ^{36}Cl/^{10}Be ratio towards the poles, in agreement with the ice core data presented in Table 1 (105). However, the authors of the modelling study hypothesised that a higher scavenging efficiency for gaseous H^{36}Cl compared to aerosol-bound ^{10}Be in mixed-phase (ice and water) clouds was responsible for the increase of the ratio (86, 87, 91, 105), which is another plausible explanation.

2.3 Chlorine loss

A second challenge for dating ice with the ^{36}Cl/^{10}Be ratio is the loss of ^{36}Cl at low accumulation sites. The issue has been studied in snow pits from Vostok in East Antarctica, where the accumulation rate is extremely low with just 2.1 g cm^{-2} yr^{-1} (28). Nuclear bomb tests in the 1950s, especially those performed on ships and small islands in 1954, 1956, and 1958, produced large quantities of anthropogenic ^{36}Cl through neutron activation of sea-salt ^{35}Cl (49, 88). Highly elevated ^{36}Cl concentrations up to a thousand times above natural levels were measured in different Antarctic and Greenland ice cores, peaking in 1958 and returning to pre-bomb levels by the mid 1980s (29, 41, 88). In Vostok, however, the peak was much broader than in other cores and shifted upwards to snow about 10 years younger. ^{36}Cl concentrations remained elevated up to the surface, corresponding approximately to the year 1997 (26). In Figure 3, the profile is compared to ^{36}Cl concentrations from Dye3 in Greenland (aligned to depths corresponding to the Vostok timescale), demonstrating the apparent mobility of ^{36}Cl.

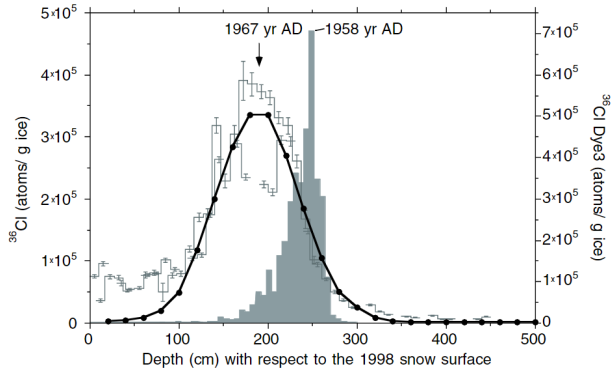

Figure 3: ^{36}Cl concentrations from a snow pit at Vostok station, East Antarctica, and modelled concentrations taking into account advective transport and diffusion (black line). ^{36}Cl concentrations from Dye3 in Greenland, corresponding to the same event, are shown in grey. Figure taken from Delmas et al. (26).

It has been hypothesised, that the deposition of ^{36}Cl, especially as H^{36}Cl gas, is reversible. The phenomenon has been researched extensively for sea-salt chlorine, which can be converted to HCl gas by acidic species, such as nitric acid (HNO_3) and sulphuric acid (H_2SO_4), during transport and after deposition (45, 53, 54, 95). In freshly emitted sea-salt, the Cl^-/Na^+ ratio by weight is 1.8 (57) and lower values indicate a chlorine loss, while higher values can indicate an excess (74). As the sea-salt flux decreases with an increasing distance from the ocean, HCl gas becomes a significant contributor to the ionic budget, leading to heightened Cl^-/Na^+ ratios in surface snow (12). However, the ratio rapidly decreases with depth, eventually reaching values below 1.8, showcasing the reversibility of HCl deposition (12, 26, 95). The process appears to be strongly related to precipitation, as the snow is buried before a re-emission of HCl can occur at sites with higher accumulation rates, where no decrease of the Cl^-/Na^+ ratio is observed in firn (95). A threshold of 4–8 g cm^{-2} yr^{-1} has been suggested for preservation (12, 81). Drill sites in Antarctica and Greenland with a well preserved ^{36}Cl bomb peak signal at the expected depth also fulfil this preservation criterium (41, 69, 88).

For ^{36}Cl/^{10}Be dating, the main potential issue related to the reversible deposition of HCl is a varying degree of unquantified ^{36}Cl loss. A rearrangement of the ^{36}Cl concentration in firn or the loss of a constant fraction would be unproblematic, but if the initially deposited ^{36}Cl/^{10}Be ratio is not preserved and the degree of ^{36}Cl loss varies

over time, the long-term variability of the measured $^{36}Cl/^{10}Be$ increases, adding to the climate related transport and deposition variability. In practice, a larger uncertainty for the estimated initial ratio would be obtained, which would translate into a larger uncertainty for age estimates, as shown in Equation 7. As a secondary effect, the loss of ^{36}Cl would increase the mass of ice needed for the measurement of the radionuclide. The issue appears to be limited to low accumulation sites, where, however, the oldest ice is often found. At EDC, where the present-day accumulation rate is 2.7 g cm^{-2} yr^{-1} (83), the so far oldest continuous ice core was drilled with a bottom age of over 800 kyr (16). The new Beyond EPICA Oldest Ice Core (BE-OIC) ice core has been estimated to reach back more than 1,200 kyr in time and has been drilled at LDC, where the present-day accumulation rate is about 2.5 g cm^{-2} yr^{-1} (15, 78). $^{36}Cl/^{10}Be$ dating may still be possible at these sites, as Röthlisberger et al. showed that sea-salt chlorine is also preserved in glacial times at EDC, even though glacial accumulation rates are even lower (81). A Cl^-/Na^+ ratio close to the sea-salt reference value of 1.8 was explained with the neutralisation of acidic species, responsible for the conversion of NaCl to HCl, with increased amounts of alkaline dust prevalent in glacial periods (81). Similarly, the dust may have neutralised H^{36}Cl gas, converting it to a less volatile species and leading to a preservation of the deposited $^{36}Cl/^{10}Be$ ratio in glacial ice. While limiting the selection of dateable samples, it would enable age estimates even at low accumulation sites.

2.4 ^{10}Be mobility

A third process which can affect the $^{36}Cl/^{10}Be$ ratio in ice is the post-depositional mobility of ^{10}Be. Anomalous behaviour has been observed in the EDC and EPICA Dronning Maud Land (EDML) ice cores from Antarctica as well as the GRIP ice core from Greenland (4, 8, 48, 73). At EDC, ^{10}Be was measured with a resolution of 11 cm in about 100 m of ice representing the time from 680 to 800 kyr BP (73). Concentration spikes up to one order of magnitude higher than in samples from adjacent depths were observed for several 11 cm pieces of ice by Raisbeck et al.. For comparison, the Matuyama-Brunhes geomagnetic field reversal investigated in the same publication only caused a ^{10}Be concentration enhancement by a factor of 2, so the spikes are unlikely to reflect changes in the production signal. Raisbeck et al. argue that the spikes rather result from a post-depositional localisation process and since smoothing over several thousand years did not remove the spikes, they concluded that the migration occurs predominantly horizontally, not from adjacent depths.

In a different approach to radionuclide dating, Auer et al. measured ^{26}Al and ^{10}Be in the EDML ice core (4). The benefit of ^{26}Al over ^{36}Cl is that its chemical behaviour is closer to that of ^{10}Be, which means it attaches to atmospheric particles as well and the $^{26}Al/^{10}Be$ ratio should be less sensitive to climatic changes affecting the radionuclides' transport and deposition. While this appears to be the case in surface snow, where the $^{26}Al/^{10}Be$ ratio remained close to its atmospheric value, the measured $^{26}Al/^{10}Be$ ratio in ice from the deepest EDML section exhibited a peak over a several thousand years and a ten-fold increase of the ^{10}Be concentration was observed in the deepest measured sample (4). Auer et al. suggested that these observations may be caused by a post-depositional mobilisation of ^{10}Be. In Greenland, a similar process has been observed in the GRIP ice core, where the fraction of dust-associated ^{10}Be increased from less than 10 % to about 50 % (8, 92).

The three drill sites, EDC, EDML, and GRIP, differ considerably in terms of their geophysical locations, impurity contents, and bottom ages. However, anomalous ^{10}Be behaviour was observed below depths of 2,700 m in all cores, suggesting that pressure and temperature may play a more critical role than the age of the ice. Near the bottom, all three cores are close to their pressure melting points. As the temperature increases near bedrock, premelting occurs: a liquid layer forms on the surface of solid ice grains even below the bulk melting point of the ice (75). This process is facilitated by the concentration of soluble impurities at grain boundaries and triple junctions, which depresses the local melting temperature. The resulting inter-granular liquid phases have been shown to be acidic and enable the mobility of various impurities (25, 34, 58, 82), possibly including ^{10}Be. Additionally, the acidic brines have been found to promote geochemical reactions and remineralisation (5), potentially leading to the formation of new beryllium compounds or the incorporation of beryllium into other minerals.

For age estimates with the $^{36}Cl/^{10}Be$ ratio, well-preserved radionuclide concentrations are crucial. A small-scale mobility and an association with dust are unproblematic, as long as the process occurs over small distances

in comparison to the sample size and ^{10}Be concentrations can still be quantitatively determined. If, however, ^{10}Be concentrations in deep ice are redistributed to a degree where it alters the initially deposited ^{36}Cl/^{10}Be ratio of a given sample, the benefit of theoretically removing the production signal may be compromised and more reliable results may be achieved with the ^{36}Cl concentration alone. If new compounds are formed and prevent the quantitative detection of ^{10}Be, the standard sample preparation methods have to be revised.

3 Methodology

3.1 Drill sites

Within the scope of this thesis, ice from three Antarctic drill sites was analysed. EPICA Dome C is located on the East Antarctic Ice Sheet at 75°05'59" S 123°19'56" E, as shown in Figure 4, at an elevation of 3,233 m. The snow accumulation rate of 2.7 g cm^{-2} yr^{-1} is extremely low at this site and the 3,260 m long ice core drilled here extends continuously to over 800 kyr BP (16, 83). We measured ^{36}Cl and ^{10}Be concentrations in discrete samples from interglacial and glacial periods with ages between 3 and 887 kyr BP to investigate the loss of ^{36}Cl, assess the variability of the ^{36}Cl/^{10}Be ratio, and compare the decrease over time to the expected radioactive decay. A second set of glacial EDC samples was analysed with the aim of better understanding post-depositional ^{10}Be mobility.

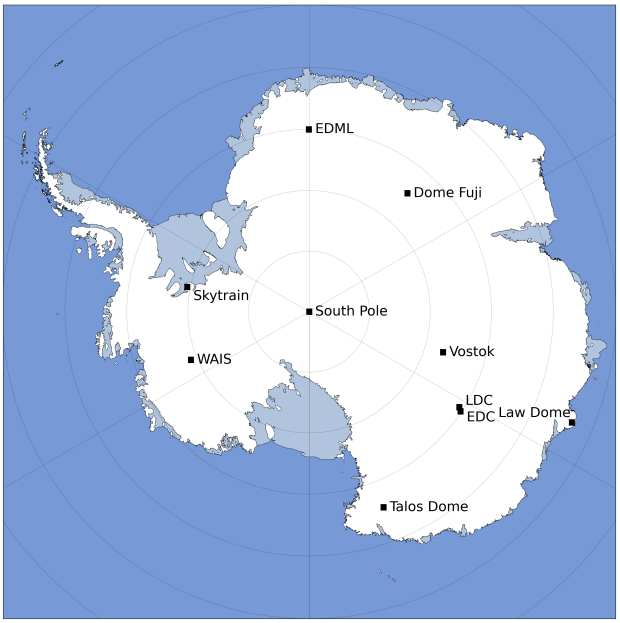

Figure 4: Antarctica with selected, relevant drill sites. The map was generated using medium resolution vector polygons of the Antarctic coastline (Version 7.10) from the SCAR Antarctic Digital Database (ADD) (35).

Additional samples were collected from Little Dome C (LDC), which is located at a distance of only 40 km from the EDC station and therefore provides very similar conditions: the accumulation rate is 2.5 g cm^{-2} yr^{-1} (78). It is also the drilling location of the Beyond EPICA Oldest Ice Core project, which has retrieved ice as old as 1.2 million years with several hundreds of meters below left undated (15). In this project, the ice of a 462 m long core from the Rapid Access Ice Drilling campaign was analysed (77). We determined the ^{36}Cl and ^{10}Be concentrations in discrete samples from the Holocene and the last glacial period to investigate the loss and preservation of ^{36}Cl.

Several measurements were also conducted on ice from an ice core drilled at Skytrain Ice Rise, which is an independent ice rise with an altitude of 784 m, located in West Antarctica, adjacent to the Ronne Ice Shelf and the West Antarctic Ice Sheet (WAIS) at 79°44'30" S 78°32'42" W (59). The 651 m deep core was drilled to assess the stability of the WAIS during the last interglacial period, when the Southern Ocean and Antarctica were warmer than today (59, 98). ^{36}Cl and ^{10}Be concentrations were analysed in continuous samples with

annual and biennial resolution from recent decades to assess the preservation of nuclear-bomb produced ^{36}Cl. Additionally, discrete samples from the Holocene and the last interglacial period were analysed and compared to different climate proxies. Then, the average initial ^{36}Cl/^{10}Be ratio was estimated and used to date five samples of unknown age below the published age scale, which extends to 126 kyr BP at a depth of 627 m (60).

3.2 Preparation of ^{36}Cl and ^{10}Be

Radionuclide concentrations were determined by adding a precisely known mass of stable isotope carrier to an ice sample and measuring the ratio of radionuclide atom counts relative to stable isotope atom counts in an accelerator mass spectrometer (AMS). For ^{10}Be, this ratio is $\frac{^{10}\mathrm{Be}}{^{9}\mathrm{Be}}$ and the concentration $c\,(^{10}\mathrm{Be})$ in atoms per gram ice can be calculated as

$$c\,(^{10}\mathrm{Be}) = \frac{m\,(^{9}\mathrm{Be}) \cdot \mathrm{N_A}}{M\,(^{9}\mathrm{Be}) \cdot m_{\mathrm{Ice}}} \cdot \frac{^{10}\mathrm{Be}}{^{9}\mathrm{Be}}, \tag{8}$$

where $m\,(^{9}\mathrm{Be})$ is the mass of added ^{9}Be carrier, $\mathrm{N_A}$ is the Avogadro constant, $M\,(^{9}\mathrm{Be})$ is the molar mass of ^{9}Be, and m_{Ice} is the mass of the ice sample. ^{36}Cl concentrations were determined in the same way using the parameters of ^{35}Cl and ^{37}Cl and adding the mass of naturally occurring chlorine in the sample to the carrier mass. While negligible at EDC, an average sea-salt chlorine mass of 3.5 % of the carrier mass was present in Skytrain samples.

All samples were prepared following the same standard procedure, with slight modifications depending on the sample type and mass, as visualised in Figure 5. First, the ice was weighed and stable isotope carrier was added, which defined the ratio of radionuclide atoms relative to stable isotope atoms. If any amount of the sample was lost in one of the preparation steps, it would not have affected the measurement outcome, as isotopic ratios, the measured parameter, would remain unchanged. Enough carrier had to be added to handle the sample, while the addition of too much carrier would have lead to larger errors from low ratios of radionuclide to stable isotope. In practice, between 0.15 and 0.30 mg of ^{9}Be carrier was added to each ^{10}Be sample and between 2.0 and 4.0 mg of ^{35}Cl and ^{37}Cl carrier was added to each ^{36}Cl sample. If several ^{10}Be samples were combined into one ^{36}Cl sample, the chlorine carrier was equally split between beryllium samples. Samples were then either melted at room temperature or in a microwave with attention being paid to temperatures not increasing more than a few degrees above the melting temperature. Most samples were prepared using ion exchange columns (IECs): each liquid sample was transferred to an individual drip bag, which was then connected to a poly-prep prefilled chromatography column with AG 50W-X8 resin (Bio-Rad Laboratories, Inc., Hercules, CA) to isolate Be. The discharge was passed on to a chlorine column, which had been prepared with AG-4X4 resin (Bio-Rad Laboratories, Inc., Hercules, CA) in advance. Beryllium and chlorine were thereby isolated from the remaining sample, which was discarded.

In a next step, beryllium columns were eluted with 25 mL of a 4 M hydrogen chloride (HCl) solution. When only ^{10}Be was of interest and the sample weighed less than 40 g, the IEC isolation and elution steps were skipped. For some of the experiments discussed in paper III, the Be solution was acidified at this point to test whether stronger leaching or particle dissolution can affect the detected ^{10}Be/^{9}Be ratio. Then, several mL of a 25 % ammonia solution were added to each sample to precipitate beryllium hydroxide ($Be(OH)_2$) at a pH > 9 over night. On the next day, the samples were centrifuged at 4,200 rpm for 20 minutes and decanted, leaving a $Be(OH)_2$ gel. 8 mL of MilliQ water was added to the gel for washing, before the sample was centrifuged again at 4,200 rpm for 20 minutes and decanted. The $Be(OH)_2$ gel was then transferred to a quartz glass and dried for 2 hours on a heating plate, before it was placed into a tube furnace and oxidised to beryllium oxide (BeO) at a temperature of 850 °C overnight. Together with about 1 mg of Niobium, the beryllium oxide was then transferred into a target and pressed into a small tablet.

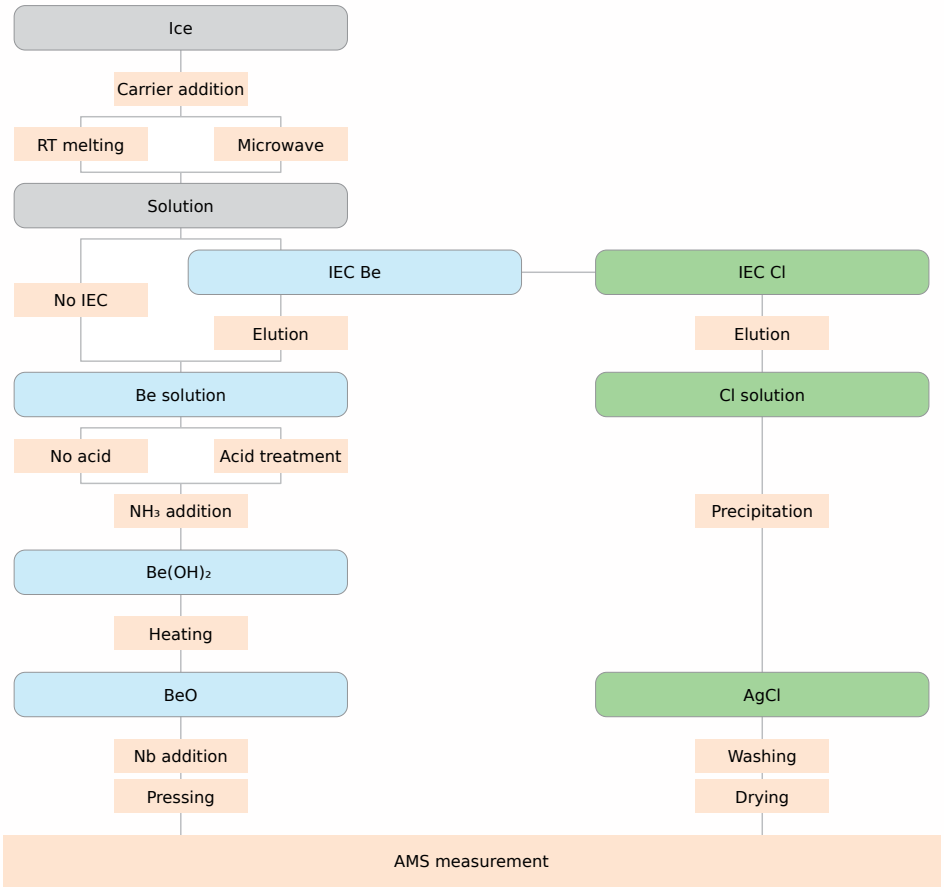

Figure 5: Overview of the radionuclide sample preparation including possible variations of the procedure for the melting of ice and the beryllium preparation.

Chlorine columns were eluded with 45 mL of a 1 M nitric acid (HNO_3) solution. To each sample, 1.0 mL of a silver nitrate ($AgNO_3$) solution with a concentration of 48 mg mL^{-1} was added and the sample was left in a dark place over night, so that silver chloride (AgCl) could precipitate. On the next day, the samples were centrifuged at 4,200 rpm for 20 minutes and decanted. The remaining silver chloride was then dissolved with 3 mL of MilliQ water and 0.5 mL of a 25 % ammonia (NH_3) solution. 1.0 mL of saturated barium nitrate ($Ba(NO_3)_2$) solution was added to precipitate barium sulphate ($BaSO_4$), as the ^{36}S isotope is an isobar to ^{36}Cl and can interfere with the measurement. The next day, the sample was centrifuged at 4,200 rpm for 20 minutes and decanted. The liquid was kept and 1.0 mL of 65 % nitric acid solution was added to re-precipitate AgCl over 2 hours before the samples were centrifuged at 4,200 rpm for 20 minutes and decanted again. To wash the samples, AgCl was re-suspended in 3.0 mL of MilliQ water, which was repeated a second time after centrifuging and decanting the samples. They were then placed in a 65 °C warm oven to fully dry for 20 hours.

Beryllium and chlorine samples were then sent to ETH Zürich, where the ratio of radionuclide to stable isotopes was determined via accelerator mass spectrometry. $^{10}Be/^{9}Be$ ratios were normalised to the ETH in-house standard S2007N with a nominal ratio of $^{10}Be/^{9}Be = (28.1 \pm 0.8) \times 10^{-12}$, which in turn was normalised against the ICN 01-5-1 standard with a nominal value of $^{10}Be/^{9}Be = 2.709 \times 10^{-11}$(21, 66). $^{36}Cl/^{35}Cl$ ratios were normalised with the in-house standard K382/4N57, which has a nominal value of $^{36}Cl/Cl = (17.36 \pm 0.34) \times 10^{-12}$ (21). The ratios were then used to calculate absolute radionuclide concentrations according to Equation 8.

3.3 Production calculations

For different purposes and on various timescales, the theoretical production rates of ^{36}Cl and ^{10}Be were calculated according to Poluianov et al. (70). The production rate P is calculated as the product of the cosmic ray energy spectrum $J_k(E_k, \phi)$, in units of sr^{-1} s^{-1} cm^{-2} with the yield function $Y(E_k, X)$, integrated over the energy spectrum from the cut-off energy $E_{\mathrm{c},k}$ to infinity as

$$P(\varphi, X, R_\mathrm{c}) = \sum_k \int_{E_{\mathrm{c},k}}^{\infty} Y_k(E_k, X) \cdot J_k(E_k, \varphi)\, \mathrm{d}E_k, \tag{9}$$

where φ is the solar modulation potential, X is the atmospheric depth, R_c is the cut-off rigidity, and E_k is the energy of cosmic ray component k. The yield functions Y are given in units of atoms g^{-1} cm^{-2} sr^{-1} and represent the number of atoms produced per gram of air at an atmospheric depth X, by primary cosmic ray component k with the unit intensity (one primary particle in interplanetary space per steradian and cm^2) (70). For the global production rate $P_\mathrm{G}(\varphi, R_\mathrm{c})$, P is integrated over the entire atmospheric depth X and the Earth's surface Ω (latitude and longitude) with

$$P_\mathrm{G}(\varphi, R_\mathrm{c}) = \frac{1}{4\pi} \int_\Omega \int_X P(\varphi, X, R_\mathrm{c}(\Omega)) \cdot \mathrm{d}X \cdot \mathrm{d}\Omega, \tag{10}$$

where $\frac{1}{4\pi}$ normalises the global production to a mean value per unit area for the spherical Earth.

For all production calculations, the yield functions were adapted from Poluianov et al. (70). For the GCR flux, the local interstellar spectrum published by Herbst et al. (43) was used as an input, modulated with different values for the solar modulation potential φ according to Equation 1. For comparisons with radionuclide data from the Skytrain ice core covering the last decades, the solar modulation potential reconstruction by Usoskin et al. (90) was used in combination with the present-day value of $M_0 = 7.8 \cdot 10^{22}$ A m^2 for the geomagnetic field (2). For comparisons with radionuclide data in the EDC ice core over the last 900 kyr, the geomagnetic field reconstruction of Channell et al. (19) (PISO-1500 stack) was used to calculate respective cut-off rigidities (see Equation 3), while a constant value of φ = 550 MV for the solar modulation potential was used for the GCR flux. For comparisons between stratospheric and tropospheric production, the average of the mean monthly tropopause pressure between 1836 and 2015 from the NOAA/CIRES/DOE 20$^{\mathrm{th}}$ Century Reanalysis (V3) dataset was used to define the latitude dependent boundary between the two atmospheric layers (84).

4 Summary of papers

This thesis is a compilation of three papers. The first one focusses on conditions enabling the preservation of ^{36}Cl at low accumulation sites and the long-term variability of the ^{36}Cl/^{10}Be ratio over the last 900 kyr. In the second paper, the climate-related variability of the ^{36}Cl/^{10}Be is analysed and the age of the previously undated bottommost 15 m of the Skytrain ice core is estimated. For the third paper, high-resolution ^{10}Be measurements in horizontal replicates and variations of the ^{10}Be sample preparation procedure were conducted to better understand the post-depositional behaviour of ^{10}Be in deep ice and ensure quantitative extraction in the future.

4.1 Paper I

Kappelt, N., Muscheler, R., Baroni, M., Beer, J., Christl, M., Vockenhuber, C., Bard, E., and Wolff, E., 2025. Ice core dating with the $^{36}Cl/^{10}Be$ ratio. Quaternary Science Reviews, 355, 109254, doi: 10.1016/j.quascirev.2025.109254.

For the first paper, we measured radionuclide concentrations from the Holocene, the last termination and the last glacial maximum in ice from LDC, a low accumulation site, where chlorine loss was expected under present day conditions. The aim was to assess the potential preservation of ^{36}Cl under glacial conditions, when higher atmospheric concentrations of alkaline dust preserved sea-salt chlorine at EDC, where the environmental conditions are similar (81). In a second series of measurements, the ^{36}Cl and ^{10}Be concentrations were measured in discrete samples from the EDC ice core with ages between 3 and 887 kyr, to assess the feasibility of dating ice with the $^{36}Cl/^{10}Be$ ratio.

At LDC, the $^{36}Cl/^{10}Be$ ratio and the Cl^-/Na^+ ratio suggest similar behaviour for ^{36}Cl and sea-salt chlorine. During the LGM, the ratios indicate a good preservation, as they remained close to their respective reference values: the production rate ratio of 0.086 for the $^{36}Cl/^{10}Be$ ratio and the sea-salt reference value of 1.8 for the Cl^-/Na^+ ratio (57, 70). Following decreasing non-sea-salt Ca^{2+}, which is a proxy for dust, lower ratios indicate a loss of ^{36}Cl and Cl^- during the last termination and in the Holocene. In the very early Holocene, the $^{36}Cl/^{10}Be$ ratio indicates a preservation of ^{36}Cl and the Cl^-/Na^+ ratio indicates an excess of Cl^-, likely due to excess HCl gas, which is reversibly deposited under present-day conditions, but may have been preserved in this period, in which the accumulation rate was slightly higher than today. The radionuclide measurements in EDC ice confirmed, that the best strategy for dating with the $^{36}Cl/^{10}Be$ ratio at low accumulation sites is to focus on glacial samples. However, even with this limitation, the radionuclide ratio varied significantly between samples, exhibiting a relative standard deviation of 33 %, which would translate to an age uncertainty of about 180 kyr according to Equation 7, not considering the measurement uncertainty of the $^{36}Cl/^{10}Be$ ratio in a hypothetically undated sample. Additionally, the ^{10}Be flux was found to decrease faster than one would expect from physical decay alone, while the ^{36}Cl decreased as fast as its physical half-life would suggest. The study inspired further research of potential correlations between the $^{36}Cl/^{10}Be$ ratio and climate proxies in the ice core record in paper II, as well as studies of potential post-depositional ^{10}Be mobility in paper III.

4.2 Paper II

Kappelt, N., Wolff, E., Christl, M., Vockenhuber, C., Gautschi, P., and Muscheler, R., 2025. 500-thousand-year-old basal ice at Skytrain Ice Rise, West Antarctica, estimated with the $^{36}Cl/^{10}Be$ ratio. Climate of the Past, doi: 10.5194/egusphere-2025-1780 (in press).

In a second study, we measured radionuclide concentrations in ice from the Skytrain ice core with the aim of reducing the dating uncertainty related to the climatic variability of the $^{36}Cl/^{10}Be$ ratio and dating five samples from below the established chronology, which extends to 126 kyr BP at a depth of 627 m (60). While the site should not be affected by chlorine loss with an accumulation rate of 13.5 $g\,cm^{-2}\,yr^{-1}$ (44), this assumption was tested by comparing the depth and shape of a nuclear bomb test related peak in the ^{36}Cl concentration from the 1950s to the signal recorded at other sites with and without ^{36}Cl loss. Radionuclide concentrations were then determined in discrete samples from the Holocene, the last glacial period and from depths between 627 m and bedrock at 651 m.

The comparison of bomb peak data showed that there is no apparent loss of ^{36}Cl at Skytrain Ice Rise, the accumulation rate is high enough to preserve the radionuclide. Without this possible interference, the influence of different climatic conditions on the $^{36}Cl/^{10}Be$ ratio was analysed and correlations with different climatic proxies were tested. Both, ^{36}Cl and ^{10}Be concentrations were correlated with the $\delta^{18}O$ signal, but with different sensitivities, hinting towards a dilution effect and an additional contribution, likely from different degrees of washout, different temperature dependent scavenging efficiencies, or both. This results in the $^{36}Cl/^{10}Be$ ratio also correlating with the $\delta^{18}O$ signal, which was used to apply a $\delta^{18}O$-based climate correction to reduce the

standard deviation of the mean initial ^{36}Cl/^{10}Be ratio from 14 to 10 % of the mean. In the five undated samples, the ^{36}Cl/^{10}Be ratio decreases steadily with depth and suggests an ice age of 552 $\pm$ 112 kyr BP about 1 m above bedrock. However, the shallowest two samples indicated ages younger than 126 kyr BP, hinting towards potential issues with post-depositional ^{10}Be processes, similar to those found at EDC in paper I, further motivating us to closer investigate the behaviour of ^{10}Be in deep ice in paper III. Based on ^{36}Cl decay alone, older age estimates were obtained, in better agreement with other dating methods (96).

4.3 Paper III

Kappelt, N., Larkman, P., Bohleber, P., Adolphi, F., Christl, M., Vockenhuber, C., Gautschi, P., Wolff, E., and Muscheler, R., 2025. Post-depositional processes of ^{10}Be in deep ice. The Cryosphere (manuscript).

Low ^{10}Be concentrations in the oldest samples from the EDC and Skytrain ice cores, as well as concentration spikes reported by Raisbeck et al. (73) inspired a closer investigation of ^{10}Be in deep ice. We analysed eight A-cuts (approximately one quarter of a 10 cm diameter core) from EDC, one from each of the eight glacial periods which occurred over the last 800 thousand years. Each A-cut was further divided into five depth intervals with seven horizontal replicates, weighing between 20 and 40 g each. The aim was to assess the horizontal variability of ^{10}Be concentrations and its potential development with increasing depth and age. Different variations of the standard sample preparation procedure were tested to investigate possible effects of acidic pre-treatment and the use of ion exchange columns in comparison to directly precipitated ^{10}Be (see Figure 5). Additionally, the grain boundary structure of one sample from each depth was analysed with a Large Area Scanning Microscope (LASM) (50) to test whether it can have an influence on the ^{10}Be concentration.

Apart from the deepest sample, the range and standard deviation of ^{10}Be concentrations among horizontal replicates showed a tentative increase, supporting a horizontal migration of ^{10}Be, as suggested by Raisbeck et al. (73). Although no spikes similar to those of Raisbeck et al. were found in our samples, a local accumulation and depletion from such a mobility seems plausible. A pre-treatment with nitric acid had no effect on ^{10}Be concentrations, the average difference to untreated samples being close to 0 at/g. It was hypothesised that an association with dust or the inclusion in newly formed compounds could prevent the quantitative analysis of ^{10}Be, but our data shows that there is no systematic impact of stronger acidic treatment, suggesting that all ^{10}Be is measured using the standard preparation procedure. Samples prepared with ion exchange columns, on the other hand, exhibited systematically lower ^{10}Be concentrations than directly precipitated samples. The relative discrepancy became larger with depth, increasing to up to 40 % at an age of of 750 kyr, approximately the amount which appeared to be missing in previous, deep EDC samples of paper I. Applying a correction to the initial ^{10}Be data based on the approximate impact of the columns results in an exponential fit to the data with a ^{10}Be half-life in agreement with the correct value of 1,387 kyr. An explanation for lower concentrations with ion exchange columns could be the association of ^{10}Be with dust, which is either not retained in columns and flushed out with the meltwater, or is retained but requires stronger elution to release ^{10}Be quantitatively. The dust associated fraction of ^{10}Be in the GRIP ice core increased from about 10 % at the surface to about 50 % at a depth of 3,000 m (92), similar to the amount lost with IECs. The analysis of the microstructure showed that even for such small samples as used in this study, the grain boundary content of adjacent samples is identical, while ^{10}Be concentrations differ, which means ^{10}Be can not be distributed homogenously along grain boundaries. In conclusion, ion exchange columns appear to lead to lower ^{10}Be concentrations in deep ice, which should be tested with ice from other drill sites as well.

Table 2 lists the contributions of all authors to the three papers included in this thesis.

Table 2: Author contributions to the papers.

Contribution	Paper I	Paper II	Paper III
Conceptualisation	N. Kappelt R. Muscheler M. Baroni E. Wolff	N. Kappelt R. Muscheler E. Wolff	N. Kappelt R. Muscheler P. Larkman P. Bohleber F. Adolphi
Data curation	N. Kappelt M. Baroni M. Christl C. Vockenhuber ASTER team	N. Kappelt M. Christl C. Vockenhuber P. Gautschi	N. Kappelt P. Larkman M. Christl C. Vockenhuber P. Gautschi
Formal analysis	N. Kappelt	N. Kappelt	N. Kappelt P. Larkman
Funding acquisition	N. Kappelt R. Muscheler M. Baroni E. Bard E. Wolff	N. Kappelt R. Muscheler E. Wolff	N. Kappelt R. Muscheler P. Bohleber E. Wolff
Investigation	N. Kappelt M. Baroni M. Christl C. Vockenhuber ASTER team	N. Kappelt M. Christl C. Vockenhuber E. Wolff	N. Kappelt P. Larkman P. Bohleber M. Christl C. Vockenhuber
Methodology	N. Kappelt R. Muscheler M. Baroni J. Beer M. Christl C. Vockenhuber ASTER team E. Wolff	N. Kappelt E. Wolff R. Muscheler	N. Kappelt P. Larkman P. Bohleber F. Adolphi R. Muscheler E. Wolff
Resources	R. Muscheler M. Baroni M. Christl C. Vockenhuber E. Bard ASTER team	E. Wolff M. Christl C. Vockenhuber P. Gautschi	P. Larkman P. Bohleber F. Adolphi M. Christl C. Vockenhuber P. Gautschi R. Muscheler
Supervision	R. Muscheler E. Wolff	E. Wolff R. Muscheler	P. Bohleber R. Muscheler E. Wolff
Visualisation	N. Kappelt	N. Kappelt	N. Kappelt P. Larkman
Writing - original draft	N. Kappelt	N. Kappelt E. Wolff	N. Kappelt P. Larkman
Writing - review & editing	All authors	All authors	All authors

5 Discussion

5.1 Loss of ^{36}Cl and climate influences

It has been suggested in different studies, that stratospheric ^{36}Cl is present in the gas phase, while ^{36}Cl produced in the troposphere attaches to aerosols, similar to ^{10}Be (41, 103, 105). Under this assumption, tropospheric and stratospheric contributions of 30 and 70 %, respectively, to the modelled ^{36}Cl deposition flux were estimated for the region from 60 to 90° S (105). At EDC, the mean ^{36}Cl/^{10}Be ratio measured in LGM ice is 0.119, close to the calculated production rate ratio 0.086 and representative of the overall atmospheric ^{36}Cl/^{10}Be ratio without ^{36}Cl loss. In recent Holocene ice (younger than 6,500 yr BP), the ratio is 0.037, 31 % of the LGM value and about the same as the tropospheric contribution to the overall flux (see Figure 6). Since aerosol attached ^{36}Cl is more likely to form salts and remain in the solid phase, it would be possible that only the ^{36}Cl of tropospheric origin is preserved in the Holocene. At LDC, the Holocene ^{36}Cl/^{10}Be ratio of 0.017 is even lower relative to the sites LGM value of 0.092, only 19 %. Acidic conversion to H^{36}Cl may further decrease the aerosol bound fraction of ^{36}Cl, similar to the processes affecting sea-salt aerosols, which are emitted with a Cl^-/Na^+ ratio of around 1.8, while the annual average Cl^-/Na^+ ratio in aerosols at EDC is 0.7, due to the acidic conversion of chloride to HCl during transport (53). Some HCl gas is deposited in the snow, causing a Cl^-/Na^+ ratio of around 6 at the surface of EDC, but the average Cl^-/Na^+ ratio in firn between a depth of 10 and 50 m is 0.58, so initially deposited HCl gas is fully re-emitted and additional conversion to HCl can occur in the firn (53, 81). Therefore, it is unlikely that dry deposition of gaseous H^{36}Cl can contribute to the recorded radionuclide signal in the

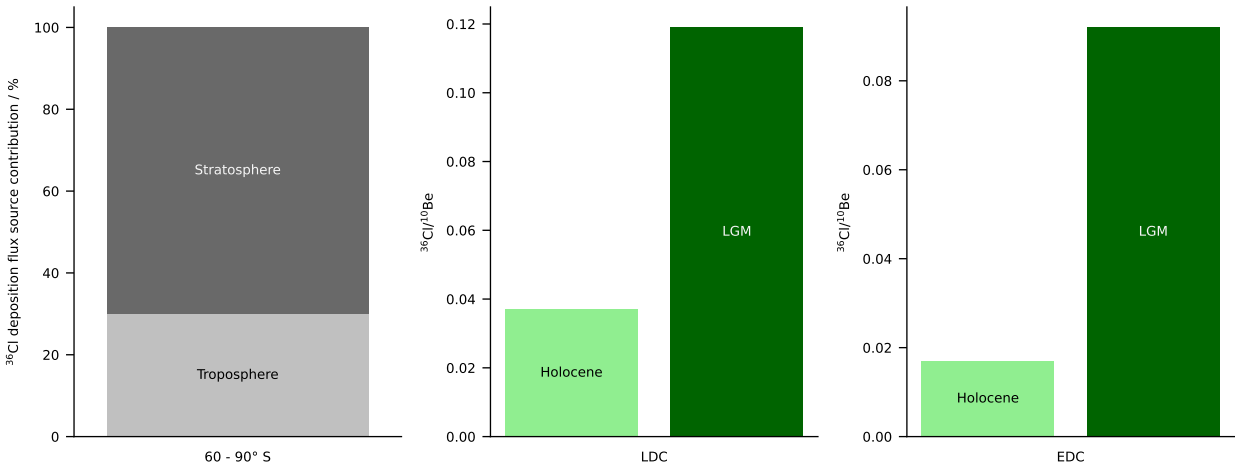

Figure 6: Comparison of the ^{36}Cl deposition flux source contributions from Zheng et al. (105) with the measured Holocene and LGM ^{36}Cl/^{10}Be ratios at LDC and EDC.

Holocene, while it has been estimated that at least 60 % of ^{10}Be is deposited dry in central Antarctica (42, 71), supporting the idea that only tropospheric ^{36}Cl is recorded in the ice. The average Cl^-/Na^+ ratio at LDC in the available dataset between a depth of 29 and 47 m is 0.56 (79), very similar to the EDC value. LDC is located at a distance of merely 40 km from EDC, the environmental conditions are very similar at the two sites, and a similar sea-salt aerosol fractionation can be expected for the local atmosphere. The preservation of ^{36}Cl would have to be very sensitive to the accumulation rate, if the lower ^{36}Cl/^{10}Be ratio in the Holocene is caused by the 8 % lower accumulation rate at LDC. In our study, only a few samples from each site were measured, limiting our ability to draw robust conclusions on the cause of the difference. To confirm whether there really is a significant difference between them, it would be helpful to analyse additional samples.

For dating with the ^{36}Cl/^{10}Be ratio, it is helpful to know whether samples need to be carefully selected to avoid those affected by ^{36}Cl loss or if the loss is predictable enough to account for it in any sample. Four parameters are of interest for this purpose. The Cl^-/Na^+ ratio is a measure of Cl^- loss, analogous to the ^{36}Cl/^{10}Be ratio as a measure of ^{36}Cl loss. The accumulation rate is the defining parameter for chlorine loss under present day conditions, used to distinguish sites with and without loss. Non-sea-salt calcium (nss-Ca^{2+}) is a proxy for atmospheric dust concentrations, which have been suggested to prevent sea-salt fractionation when sufficiently high. The water isotopic signature is considered an overall climate signal and is tightly linked to both, the accumulation rate and nss-Ca^{2+} concentrations. Figure 7 demonstrates the relationship between the different parameters over the entire EDC core. As described by Röthlisberger et al. (81), high nss-Ca^{2+} concentrations provide the conditions for a stable Cl^-/Na^+ ratio close to the sea-salt reference value of 1.8. A gradual decrease of the ratio towards lower nss-Ca^{2+} concentrations can be observed below 20 µg kg^{-1} in cold climates. For very low nss-Ca^{2+} concentrations in warm periods with higher accumulation rates, the scatter becomes very large and the Cl^-/Na^+ ratio is rather unpredictable, especially for δD values higher than -400 ‰.

A similar behaviour is observed for the ^{36}Cl/^{10}Be ratio. The Eemian is the previous interglacial period, was warmer than the Holocene, and ice from this period contains the highest isotope ratios and accumulation rates of the record. Looking at correlations with different parameters, the data points from the Eemian appear to disrupt all trends which are present for lower isotope values, so samples with δD values higher than -400 ‰ were excluded from the correlation analysis. A correlation between the ^{36}Cl/^{10}Be ratio and the deuterium signal at LDC is also observed only for δD values lower than -390 ‰. The deuterium signal is strongly intertwined with the accumulation rate and the nss-Ca^{2+} concentration, but correlates with the ^{36}Cl/^{10}Be ratio the strongest out of the three parameters at EDC. The correlation is a likely combination of two effects: the transport and deposition related increase of the ^{36}Cl/^{10}Be ratio and the increasing preservation of ^{36}Cl in colder climates. Also at sites without ^{36}Cl loss, like Skytrain and GRIP (101), higher ^{36}Cl/^{10}Be ratios are observed in glacial periods compared to interglacial periods, which may be linked to a decreasing scavenging efficiency for ^{10}Be in mixed phase clouds,

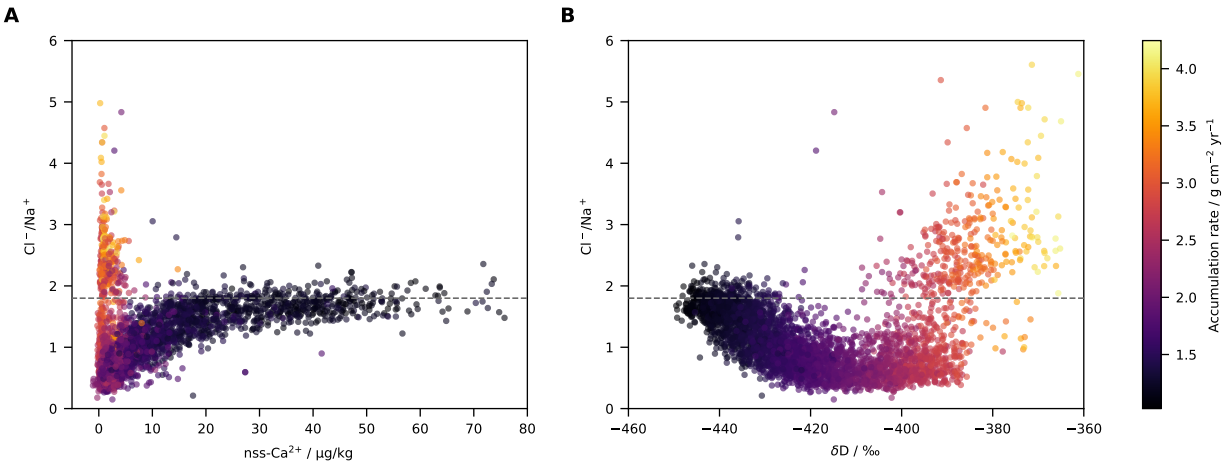

Figure 7: Relationship of the Cl^-/Na^+ ratio with **A** the nss-Ca^{2+} concentration, **B** the deuterium signal and the accumulation rate (colour coded) in the EDC ice core over the last 800 kyr, using chemistry data from Wolff et al. (97), deuterium data from Jouzel et al. (46), and accumulation data from Bouchet et al. (16). The dashed line marks the reference value of freshly emitted sea-salt, 1.8 (57).

which are more prevalent in cold periods, while ^{36}Cl scavenging remains consistently high (27, 86, 87, 105). However, at EDC, the $^{36}Cl/^{10}Be$ ratio is much more sensitive to changes in the deuterium signal, as the slope of a linear fit to the data is about six times higher than at Skytrain (see Figure 8), likely due to the additional ^{36}Cl preservation contribution.

For ^{10}Be, the negative correlation of the concentration with the accumulation rate and the positive correlation of the flux with the accumulation rate are consistent with a dry deposition fraction of about 60 %, as suggested by Raisbeck and Yiou and Heikkilä et al. (42, 71), and a lower scavenging efficiency in mixed phase clouds. For ^{36}Cl, however, both, the concentration and the flux, are negatively correlated with the accumulation rate. It is possible, that the dry deposition fraction increases towards colder climates over the entire range of δD values, as more stratospheric $H^{36}Cl$ gas is converted to salts, which can be irreversibly deposited. This would suggest that a measured $^{36}Cl/^{10}Be$ ratio close to the production rate ratio does not necessarily indicate a complete preservation of ^{36}Cl at EDC, but rather results from the combined increased ^{36}Cl concentrations and decreased ^{10}Be concentrations in a colder climate. A good correlation also exists between the $^{36}Cl/^{10}Be$ ratio and the Cl^-/Na^+ ratio ($r = 0.67$, $p < 0.001$). A linear fit to the data shows that the $^{36}Cl/^{10}Be$ production rate ratio of 0.086 is reached at a Cl^-/Na^+ ratio of 0.92, when significant amounts of sea-salt chlorine are still lost, making incomplete ^{36}Cl preservation despite at $^{36}Cl/^{10}Be$ ratio of 0.086 likely. The $^{36}Cl/^{10}Be$ ratio of 0.12 reached at a

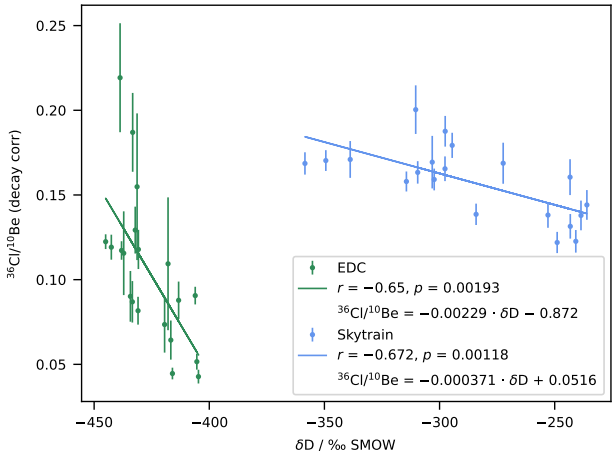

Figure 8: Comparison of the correlations between the decay corrected $^{36}Cl/^{10}Be$ ratios from EDC and Skytrain with the deuterium signal. Isotope data are published in (46) and (60).

Cl^-/Na^+ ratio of 1.8, indicating complete sea-salt chlorine preservation, is more likely to represent a complete preservation of ^{36}Cl as well. Due to the cold climate, it is higher than the production rate ratio at EDC.

5.2 Detrending radionuclide data

The relationship with δD can be used to detrend the ^{36}Cl/^{10}Be ratio at EDC without distinguishing between loss and transport/deposition effects. Analogous to the methodology of paper II, where this was applied to data from Skytrain, predicted ^{36}Cl/^{10}Be ratios and ^{36}Cl concentrations are calculated based on the linear relationships shown in Figure 9, panels A and C. The decay corrected measured ^{36}Cl/^{10}Be ratio and ^{36}Cl concentration are then divided by the predicted values, reducing the variability as shown in Figure 9, panels B and D. The variability of the ^{36}Cl/^{10}Be ratio at EDC is larger than at Skytrain, as shown in Table 3, but the one-sigma standard deviation from the mean is significantly reduced from 0.43 to 0.32 through detrending. This is useful for reducing the uncertainty of age estimates (5.5 kyr per percentage point, see Equation 7), but detrending the ^{36}Cl concentration and flux with the deuterium signal yields even lower relative standard deviations of 0.28 and 0.27, respectively. The reduction is larger for the concentration (see Table 3), since calculating the flux already transforms the data in a similar way. Detrended, both datasets are almost identical (R^2 = 0.982). The 28 % variability of the detrended ^{36}Cl concentration is similar to the variability of the calculated production rate based on the geomagnetic field reconstruction by Channell et al. (19), which has a standard deviation of 22 % from the mean over the last 800 kyr, suggesting that the remaining variability of the detrended signal is dominated by production rate variability.

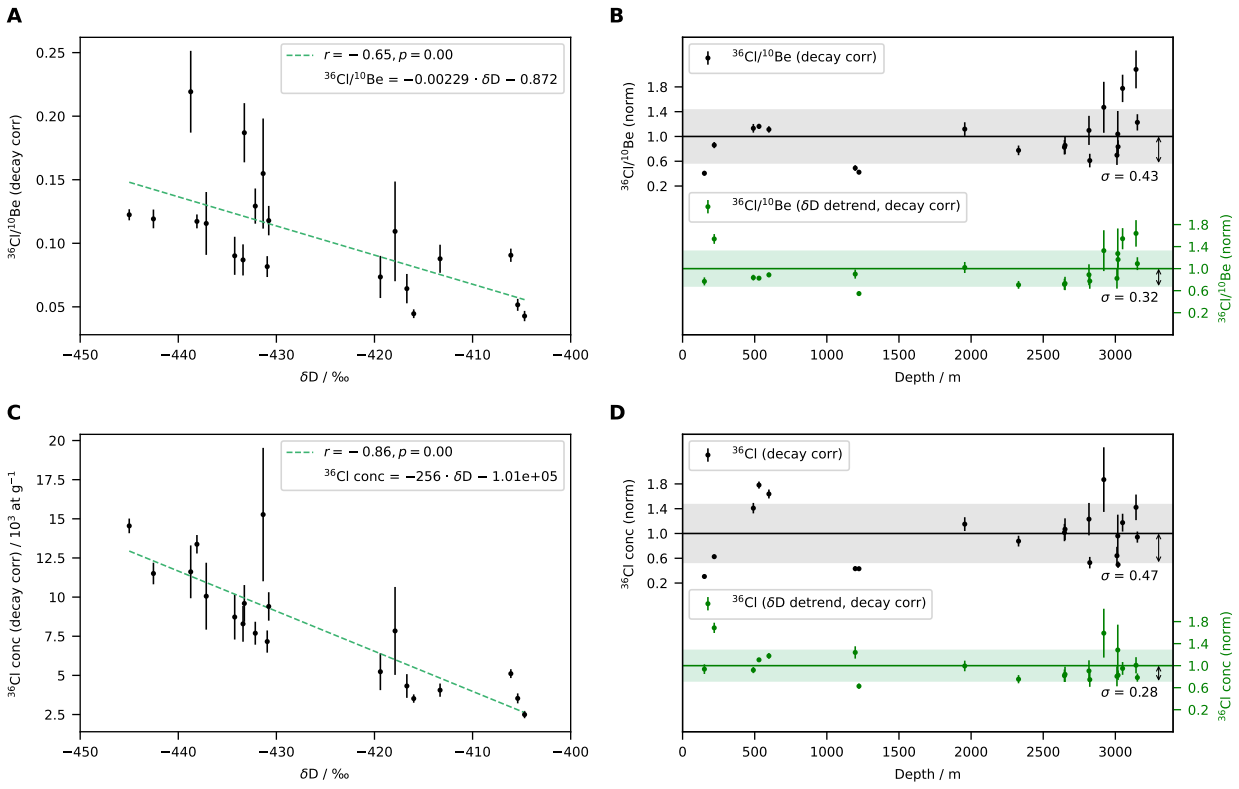

Figure 9: Radionuclide detrending at EDC. **A** and **C**: Correlation of the the δD signal with the decay corrected ^{36}Cl/^{10}Be ratio and ^{36}Cl concentration, respectively. **B** and **D**: Comparison of the variability before and after detrending of the decay corrected ^{36}Cl/^{10}Be ratio and ^{36}Cl concentration, respectively.

The lower variability of the detrended ^{36}Cl concentration means that the ^{36}Cl/^{10}Be ratio offers no improvement over ^{36}Cl alone at EDC, but would instead yield age estimates with a larger uncertainty. Even with the same relative standard deviation, lower age uncertainties would be achieved, which is evident from the full Gaussian error propagation of Equation 6. Shortening the ^{36}Cl/^{10}Be ratio to R, the age uncertainty $\sigma(t)$ is calculated as

Table 3: Standard deviations relative to the mean for different isotope ratios and datasets, including variants with deuterium detrending and/or applied weights (subscript w) based on the the represented time period (discussed in section 5.3).

	EDC			Skytrain	
	^{36}Cl/^{10}Be	^{36}Cl conc	^{36}Cl flux	^{36}Cl/^{10}Be	^{36}Cl
$\boldsymbol{\sigma}$	0.43	0.47	0.33	0.14	0.47
$\boldsymbol{\sigma}_{\boldsymbol{\delta D}\text{ detrend}}$	0.32	0.28	0.27	0.09	0.17
$\boldsymbol{\sigma}_{\text{w}}$	0.39	0.37	0.29	0.09	0.24
$\boldsymbol{\sigma}_{\boldsymbol{\delta D}\text{ detrend, w}}$	0.28	0.24	0.25	0.09	0.15
$\boldsymbol{R}_{0,\text{ w}}/\boldsymbol{R}_0$	1.18	1.02	1.02	1.12	1.26
$\boldsymbol{R}_{0,\,\boldsymbol{\delta D}\text{ detrend, w}}/\boldsymbol{R}_{0,\,\boldsymbol{\delta D}\text{ detrend}}$	1.13	0.960	0.993	1.08	1.08

$$\begin{aligned}\sigma(t) &= \sqrt{\left(\frac{\partial t}{\partial R}\sigma(R)\right)^2 + \left(\frac{\partial t}{\partial R_0}\sigma(R_0)\right)^2 + \left(\frac{\partial t}{\partial k}\Delta k\right)^2} \\ &= \sqrt{\left(\frac{1}{kR}\sigma(R)\right)^2 + \left(\frac{1}{kR_0}\sigma(R_0)\right)^2 + \left(\frac{1}{k^2}\ln\left(\frac{R}{R_0}\right)\Delta k\right)^2},\end{aligned} \tag{11}$$

where k is the decay constant. For ^{36}Cl, R and R_0 need to be substituted for the concentration $c\,(^{36}\text{Cl})$ and the estimated initial concentration $c_0\,(^{36}\text{Cl})$, respectively. In Figure 10, the calculated age uncertainties are plotted against the relative uncertainty of the initial ^{36}Cl/^{10}Be ratio R_0 and initial ^{36}Cl concentration $c_0\,(^{36}\text{Cl})$ for three different ages. The measurement uncertainties were estimated as explained in the supplement of paper I with updated AMS efficiencies of $24 \cdot 10^{-4}$ and $9.2 \cdot 10^{-4}$ for ^{36}Cl and ^{10}Be, respectively, and for a sample mass of 800 g. Since the uncertainty of the decay constant, $\Delta k = 1.5$ kyr (3), is negligible, the y-intercept is determined by the relative measurement uncertainty of the ratio $\sigma(R)$ or the ^{36}Cl concentration $\sigma(c\,(^{36}\text{Cl}))$. This will always be larger for the ratio, since $\sigma(R)/R \geq \sigma(c\,(^{36}\text{Cl}))/\,c\,(^{36}\text{Cl})$ and $k_\text{R} < k_{^{36}\text{Cl}}$. The relative uncertainty of the initial ratio $\sigma(R_0)/R_0$ or concentration $\sigma(c_0\,(^{36}\text{Cl}))/\,c_0\,(^{36}\text{Cl})$ (relative σ in Figure 10) also has a stronger influence on age estimates with the ratio, as the uncertainty scales with $1/k$ and the effective half-life of 384 kyr for the ratio is longer than the half-life of 301 kyr for ^{36}Cl alone. In the EDC ice core, age estimates are, therefore, more precise when calculated with the ^{36}Cl concentration rather than with the ^{36}Cl/^{10}Be ratio. Additionally, potential issues with ^{10}Be in deep ice are avoided when not using the ratio.

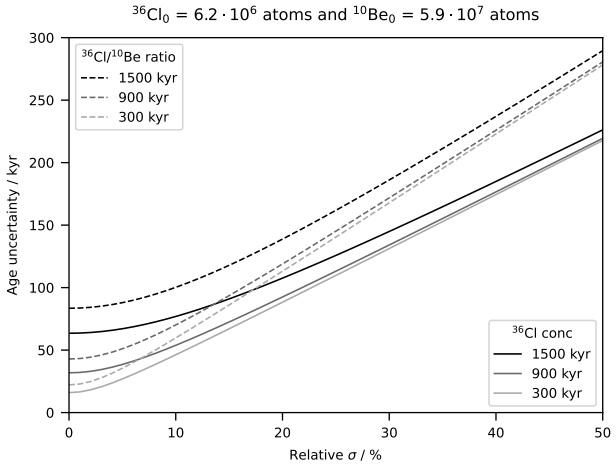

Figure 10: Age estimate uncertainties depending on the uncertainty of the initial ^{36}Cl/^{10}Be ratio or initial ^{36}Cl concentration (σ) for different ages calculated with Equation 11 and radionuclide concentrations representative of 800 g EDC ice.

At Skytrain, detrending the ^{36}Cl concentration with the deuterium signal strongly reduces the standard deviation from 0.47 to 0.17. Again, the standard deviation is similar to the calculated production rate variability based on

the geomagnetic field reconstruction by Channell et al. (19), which has a standard deviation of 15 percent from the mean over the last 126 kyr, corresponding to the time period of the well-dated Skytrain dataset. The standard deviation of the detrended ^{36}Cl/^{10}Be ratio of 0.09 is even lower, so age estimates benefit from a significant uncertainty reduction through the production signal correction that the ratio provides at this site, although the effect is dampened due to the factors discussed in reference to Figure 10. With the deuterium detrended ^{36}Cl concentration, however, all but one age estimate are older than with the ratio, all ages are older than 126 kyr BP, the oldest age of the established ST22 chronology, and the estimates are in better agreement with independent ^{81}Kr and ^{40}Ar derived age estimates (98). At this point, the confidence in purely ^{36}Cl derived ages is therefore higher than those obtained with the ^{36}Cl/^{10}Be ratio, especially for samples whose ^{10}Be content was extracted using ion exchange columns.

5.3 The influence of temporal resolution

Whether the ^{36}Cl/^{10}Be ratio or the ^{36}Cl concentration is used, the mean value of the decay corrected data of known age is used to estimate the initial value, while the standard deviation serves as an estimate of the uncertainty. However, the standard deviation depends on the temporal resolution, which is arbitrary. High resolution data could depict short-term weather effects or production rate changes related to the solar magnetic field, which are not relevant on longer timescales. A comparison of the annually resolved ^{36}Cl/^{10}Be ratio from recent decades with older data in Figure 11 demonstrates this well: the standard deviation of the high-resolution data is more than twice as high ($\sigma = 0.046$) as the standard deviation of the deeper data with lower resolution ($\sigma = 0.021$).

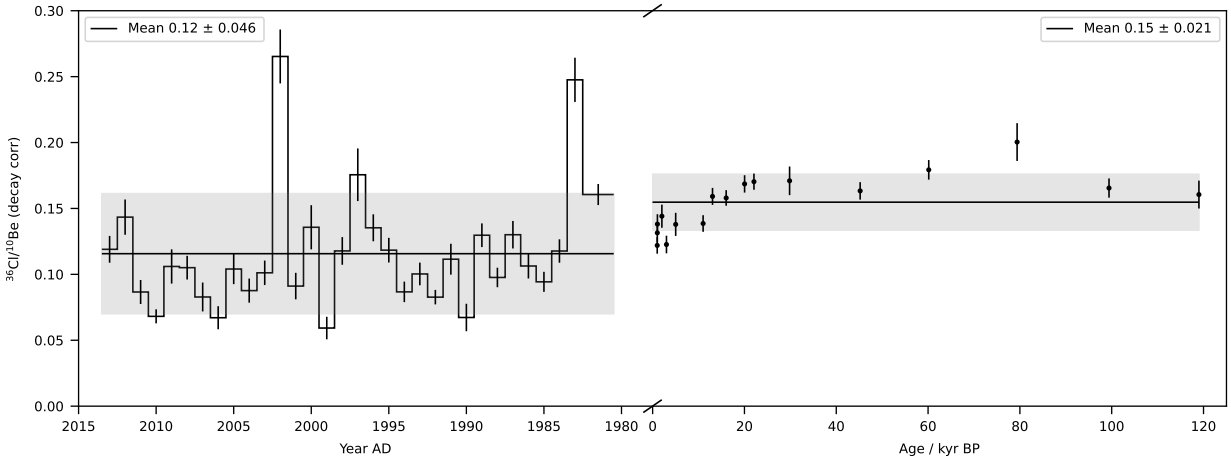

Figure 11: Comparison of the ^{36}Cl/^{10}Be ratio from recent decades with data from the last 126 kyr in the Skytrain ice core. Note the break in the x-axis and the change in time scale from calender years to kilo-years before present.

The EDC and Skytrain radionuclide datasets are discontinuous with large temporal gaps between measurements, but to estimate the influence of the resolution on the standard deviation, the reconstructed ^{36}Cl production rate based on the geomagnetic field reconstruction by Channell et al. (19) can be analysed. It would represent an idealised scenario without climatic influences and a continuously measured signal. With the published resolution of 1 kyr, the relative standard deviation from the mean is 22 % over the last 813 kyr (EDC timeframe) and 15 % over the last 126 kyr (Skytrain timeframe). A lower resolution can be simulated by binning the data into increasingly wider time intervals and averaging the production rates within each bin. The resulting relative standard deviation for different sampling resolutions is shown in Figure 12 for the EDC and Skytrain timeframes. While the mean remains unchanged in this approach, the standard deviation depends on the exact bin alignment. The starting point was, therefore, shifted in 1 kyr increments to calculate all possible configurations for a given resolution. The minimum and maximum possible standard deviations define the shaded areas shown in Figure 12. The decrease of the standard deviation with lower resolutions is substantial. For example, lowering the resolution from 1 to 30 kyr within the Skytrain timeframe cuts the uncertainty in half, from 15 % to 7 %, which would imply a reduction of the age uncertainty from 67 to 33 kyr for a 188 kyr old sample (see also Figure 10). This example describes

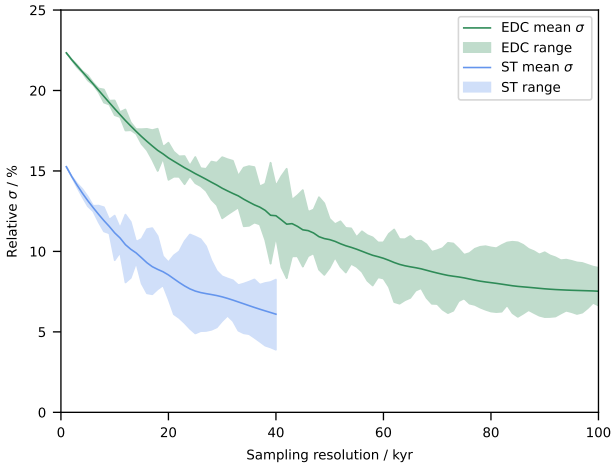

Figure 12: Theoretical impact of the temporal resolution on the relative standard deviation of the reconstructed ^{36}Cl production rate based on the geomagnetic field reconstruction of (19) over the time period of the Skytrain ice core (5–126 kyr BP, blue) and EDC ice core (5–813 kyr BP, green).

the Skytrain sample at a depth of 637 m, whose age was estimated with the deuterium detrended ^{36}Cl concentration. The age range within the sample can be estimated by fitting an exponential function to the five samples and calculating the age difference between the top and bottom depth of each sample, which is shown in Figure 13. The estimate suggests that the time period contained in the approximately 1.6 m long samples rapidly increases from 21 to 119 kyr. Uncertainty estimates based on the variability observed with a resolution of 1 kyr would, therefore, likely overestimate the age uncertainty.

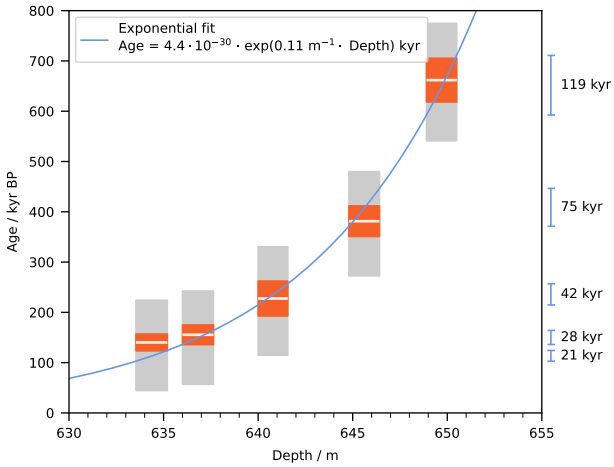

Figure 13: An exponential fit to the deuterium detrended ^{36}Cl age estimates (paper II supplementary information) was used to calculate the age difference between the top and bottom depth of each deep Skytrain ice core sample. Orange bars indicate the one-σ measurement uncertainty while grey errorbars indicate the combined measurement uncertainty and initial value uncertainty.

Unfortunately, the Skytrain and EDC datasets are discontinuous, so the resolution can not be adjusted. Downsampling to a resolution of 119 kyr would also not be possible, since the entire well-dated section at Skytrain is only 126 kyr old. Instead, the varying temporal resolution can be taken into account when calculating the mean and the standard deviation by weighting the samples based on the time period they represent. For values of the decay corrected ^{36}Cl/^{10}Be ratio R_i, measured in ice samples i representing time periods (bottom minus top age) $t_{R,i}$, the weighted mean $R_{0,\mathrm{w}}$ and standard deviation $\sigma(R_{0,\mathrm{w}})$ can be calculated as

$$R_{0,\mathrm{w}} = \frac{\sum_i t_{R,i}\, R_i}{\sum_i t_{R,i}} \tag{12}$$

and

$$\sigma(R_{0,\mathrm{w}}) = \sqrt{\frac{\sum_i t_{R,i} \left(R_i - R_{0,\mathrm{w}}\right)^2}{\sum_i t_{R,i}}}, \tag{13}$$

respectively. Outliers representing only a short time period of radionuclide deposition are given less weight, while sample representing a long time period are given more weight. This also introduces a bias, as glacial samples with lower accumulation rates and deeper samples with a lower temporal resolution are given more weight, so it needs to be applied carefully. Table 3 shows how this affects the mean relative to the mean without weighting as well as the standard deviations of different decay corrected radionuclide parameters. At EDC, both, the mean ^{36}Cl concentration and flux are barely affected by applying weights, with and without deuterium detrending. This seems counter-intuitive, as glacial samples with lower accumulation rates and higher radionuclide concentrations are given more weight than interglacial samples. However, most samples from EDC are glacial samples, which were selected to avoid interference from ^{36}Cl loss, especially in the older half of the core. The mean ^{36}Cl/^{10}Be ratio, on the other hand, increases with applied weights, which is driven by low ^{10}Be concentrations in the deepest part of the core; applying weights to the deuterium detrended ^{10}Be concentration returns a 11 % lower mean value, once again showing that using the ratio at EDC is problematic in the deepest section, at least for the samples potentially suffering from ^{10}Be loss due to the extraction with ion exchange columns (see paper III). The standard deviation decreases slightly for all radionuclide parameters at EDC, which means that weighting can improve the uncertainty of age estimates by limiting the influence of values, which deviate further from the mean but only represent a short time period. As the lowest uncertainty is achieved with the deuterium detrended and weighted ^{36}Cl concentration, this parameter can be used to test the reliability of age estimates at EDC. Estimates for the age of samples older than 600 kyr BP based on the mean decay corrected value of younger samples are shown in Figure 14. While the uncertainties are large, all estimates are in agreement with the established AICC2023 chronology (16).

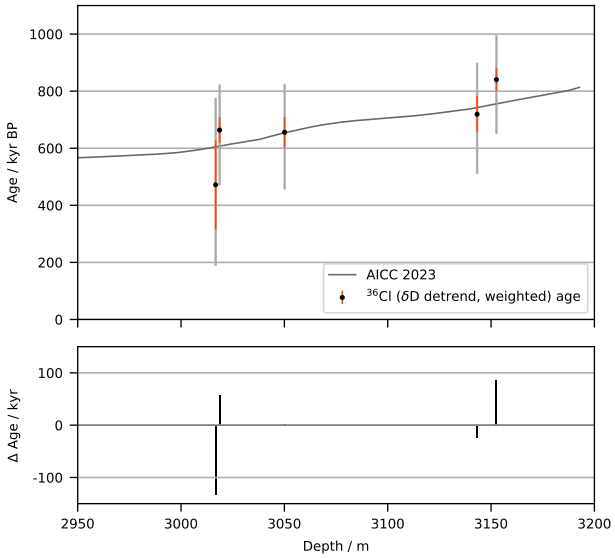

Figure 14: Estimated ages of the radionuclide samples older than 600 kyr BP at EDC in comparison with the AICC2023 age scale (16). Ages were estimated using the δD detrended ^{36}Cl concentration with the decay corrected and weighted mean ^{36}Cl concentration between 0 and 600 kyr BP as the estimated initial concentration c_0 (^{36}Cl). Uncertainties were estimated with the one-σ standard deviation analogous to the methodology of paper II.

At Skytrain, weighting significantly increases the mean ^{36}Cl/^{10}Be ratio and ^{36}Cl concentration, which is expected as the well-dated ice core only extends to 126 kyr BP and weighting by resolution therefore strongly favours glacial samples. As the deepest deuterium detrended ^{36}Cl/^{10}Be ratios and ^{36}Cl concentrations are among the highest of the dataset, a slight increase is also observed in the detrended data, as shown in Table 3. Without deuterium detrending, the weighting results in a lower standard deviation due to the low impact of Holocene data and a

lower variability among glacial data in comparison to the whole dataset. After detrending, the weighting has very little influence on the standard deviation, reflecting the overall more stable conditions at Skytrain. This means the uncertainty would remain the same, but age estimates would become slightly older with weighting, due to the elevated mean initial value. In the case of the $^{36}Cl/^{10}Be$ ratio, this would make estimates for the shallowest two samples more reasonable, as they increase from 48^{+74}_{-78} kyr and 110^{+78}_{-82} kyr to 84^{+70}_{-74} kyr and 146^{+74}_{-77} kyr, respectively.

5.4 Comparison to other dating methods

The decay of ^{36}Cl or the $^{36}Cl/^{10}Be$ ratio is not the only option for obtaining independent age estimates for old ice. Similar methods using other radionuclides have been tested or are under development and can be compared to ^{36}Cl and ^{10}Be in terms of the required sample mass and uncertainty.

The $^{26}Al/^{10}Be$ ratio has been proposed as an alternative to the $^{36}Cl/^{10}Be$ ratio, as it benefits from the chemical similarity of Al and Be. Both metals attach to aerosols in the atmosphere, while ^{36}Cl is also present in the gas phase, so the $^{26}Al/^{10}Be$ ratio in the deposition flux should be less variable and climate-dependent. Indeed, the $^{26}Al/^{10}Be$ ratio measured in atmospheric samples from different locations and in firn from four Antarctic locations deviated no more than 5 % from the mean (4). The half life of ^{26}Al is 717 kyr, so it is suited for an older age range than ^{36}Cl, but its atmospheric production rate is about 20 times lower than that of ^{36}Cl (4, 70), so several kilograms of ice are required for a measurement. In a pilot study, Auer et al. (4) determined the $^{26}Al/^{10}Be$ ratio in drill chips from the EPICA EDML ice core drilled at Kohnen station. The depth range of 2,554–2,760 m lies below the established chronology, which extends to an age of 150 kyr at a depth of 2,400 m (80). The ratio varied significantly with depth and exhibited a peak spanning over several samples, corresponding to several thousand years. Auer et al. concluded that perturbations of ^{26}Al in deep ice could be responsible for the unexpected concentrations, similar to the mobility that has been suggested to alter ^{10}Be concentrations, but without keeping $^{26}Al/^{10}Be$ ratios constant. While it should be tested whether similar behaviour is observed in other ice cores, the results suggest that the advantage of a lower variability due to chemical similarity is lost in deep ice, while requiring more ice to be measured.

A well-suited radionuclide for ice core dating is ^{81}Kr with a half-life of 229 kyr (6, 55). As a noble gas, it is inert and has a long atmospheric lifetime, so it is globally well-mixed and insensitive to short-term production variability (102). Changes to the atmospheric abundance are small and slow compared to ^{36}Cl, ^{26}Al, and ^{10}Be, which are removed from the atmosphere within years (40, 41, 88). To account for these changes, the isotopic abundance of the past can be estimated based on geomagnetic field reconstructions (17, 102). While susceptible to uncertainties of the geomagnetic field reconstruction, the reaction cross sections and the half-life of ^{81}Kr, the correction based on the calculated abundance is smaller than 4 % and the calculated present-day value agrees with measurements of modern air (17, 102). Without the variability that complicates dating with the other radionuclides, the main source of the age estimate uncertainty is the measurement uncertainty, but recent advancements in the detection method using Atom Trap Trace Analysis (ATTA) significantly reduced uncertainties as well as the required sample mass. Due to the low abundance of ^{81}Kr, the method was first tested using 350 kg of Antarctic blue ice (dense, ancient ice exposed at the surface by wind ablation) samples, but quickly developed to work with just a few kilograms of ice, for example using deep ice from the Talos Dome ice core, where three approximately 400 kyr old samples were dated with uncertainties of 9 to 16 % (23). ^{81}Kr was also used to extend the EDC age scale; the lowest of three samples weighed 6.4 kg and its estimated age was 887 kyr BP with a 10 % uncertainty (16). With further improvement of the ATTA system, ^{81}Kr can now be measured in just 1 kg of ice (76). For comparison, 600 to 900 g of ice were used to measure ^{36}Cl in deep EDC samples for paper I and about half as much ice is needed now, as a new AMS ion source at ETH Zurich allows for more efficient sample consumption.

Another method for obtaining independent age estimates is based on the increasing abundance of atmospheric ^{40}Ar, which is a decay product of ^{40}K and continuously gasses out from the Earth's crust and mantle. In a study with the aim of determining the rate of increase, the $^{40}Ar/^{38}Ar$ ratio relative to modern air $\delta^{40/38}Ar$ was determined in ice samples of the last 800 kyr weighing between 200 and 500 g (13). Plotting $\delta^{40/38}Ar$ against

the age, a regression line with a slope of (-0.066 ± 0.007) ‰/Myr gave the best fit to the data, which translates to an age estimate uncertainty of 11 %. However, a reproducibility of 0.012 ‰ was determined from the one-σ standard deviation of 15 Holocene samples, which equates to a minimum uncertainty of 180 kyr and applies to the entire age range used for calibration (13). For discontinuous blue ice up to 2.7 Myr old, ^{40}Ar dating has been proven useful (99).

If possible, it is ideal to combine different dating methods to obtain the most reliable age estimates, especially since gasses and dissolved radionuclides can often be measured in the same sample. However, gas measurements are not always possible, if the quality of the ice is poor, while ^{36}Cl and ^{10}Be can still be measured in most cases.

6 Conclusions

We were able to show that old ice can be dated with the decay of the ^{36}Cl/^{10}Be ratio, which enables the interpretation of otherwise inaccessible data in the deepest sections of ice cores, where traditional dating methods can no longer be applied. Three key challenges were addressed in this thesis.

The initial ^{36}Cl/^{10}Be ratio of a sample at the time of deposition can only be estimated, the best guess being the mean decay-corrected ^{36}Cl/^{10}Be ratio in samples of known age. The standard deviation can be large, as the transport and deposition of both, ^{36}Cl and ^{10}Be are influenced by the climate. By applying a δD- or δ^{18}O-based climate correction, it was possible to reduce the standard deviation and, therefore, the uncertainty of age estimates for the EDC and Skytrain ice cores. An additional reduction can be achieved by weighting individual data points by the time period they represent, but attention needs to be paid to avoid introducing potential bias.

While ^{36}Cl loss was initially assumed to be a major issue, it has been found to be of little relevance to the dating method. The linear relationship between deuterium and the ^{36}Cl/^{10}Be ratio holds up over almost the entire range of δD values, extending far into the regime of interglacial ^{36}Cl loss, which means it is captured by the climate correction. Larger uncertainties at EDC compared to Skytrain are rather caused by the overall higher variability of the ^{36}Cl/^{10}Be ratio at this site.

The third challenge for ^{36}Cl/^{10}Be dating is that ^{10}Be concentrations appear to decrease faster with age than possible through radioactive decay alone, as demonstrated by an underestimated half-life of an exponential fit to the EDC ^{10}Be data and overall younger ages at Skytrain with the ^{36}Cl/^{10}Be ratio compared to ^{36}Cl alone. Direct comparisons between directly precipitated ^{10}Be with samples passed through ion exchange columns showed a systematic and depth dependent ^{10}Be deficit in samples passed through columns, which is how previous EDC and Skytrain samples were treated. Depending on the variability of ^{36}Cl compared to the ^{36}Cl/^{10}Be ratio, however, using ^{36}Cl alone may still yield more precise estimates.

While uncertainties for ^{36}Cl/^{10}Be or ^{36}Cl dating are large in comparison to the continuous AICC2023 or ST22 chronologies, alternative methods for absolute dating, such as ^{81}Kr and ^{40}Ar dating, yield estimates with a similar precision and need similar masses of ice. Basal ice core sections of unknown age in Greenland and Antarctica could best be dated using all three methods. However, the advantage of the ^{36}Cl/^{10}Be ratio is that it does not require gas extraction, which can become difficult if the ice quality is poor.

7 References

[1] F. Adolphi and R. Muscheler. Synchronizing the Greenland ice core and radiocarbon timescales over the Holocene-Bayesian wiggle-matching of cosmogenic radionuclide records. *Climate of the Past*, 12:15–30, 1 2016. doi:10.5194/cp-12-15-2016.

[2] P. Alken, E. Thébault, C. D. Beggan, H. Amit, J. Aubert, J. Baerenzung, T. N. Bondar, W. J. Brown, S. Califf, A. Chambodut, A. Chulliat, G. A. Cox, C. C. Finlay, A. Fournier, N. Gillet, A. Grayver, M. D. Hammer, M. Holschneider, L. Huder, G. Hulot, T. Jager, C. Kloss, M. Korte, W. Kuang, A. Kuvshinov, B. Langlais, J.-M. Léger, V. Lesur, P. W. Livermore, F. J. Lowes, S. Macmillan, W. Magnes, M. Mandea, S. Marsal, J. Matzka, M. C. Metman, T. Minami, A. Morschhauser, J. E. Mound, M. Nair, S. Nakano, N. Olsen, F. J. Pavón-Carrasco, V. G. Petrov, G. Ropp, M. Rother, T. J. Sabaka, S. Sanchez, D. Saturnino, N. R. Schnepf, X. Shen, C. Stolle, A. Tangborn, L. Tøffner-Clausen, H. Toh, J. M. Torta, J. Varner, F. Vervelidou, P. Vigneron, I. Wardinski, J. Wicht, A. Woods, Y. Yang, Z. Zeren, and B. Zhou. International Geomagnetic Reference Field: the thirteenth generation. *Earth, Planets and Space*, 73:49, 12 2021. doi:10.1186/s40623-020-01288-x.

[3] G. Audi, F. G. Kondev, M. Wang, W. J. Huang, and S. Naimi. The NUBASE2016 evaluation of nuclear properties. *Chinese Physics C*, 41, 2017. doi:10.1088/1674-1137/41/3/030001.

[4] M. Auer, D. Wagenbach, E. M. Wild, A. Wallner, A. Priller, H. Miller, C. Schlosser, and W. Kutschera. Cosmogenic 26Al in the atmosphere and the prospect of a 26Al/10Be chronometer to date old ice. *Earth and Planetary Science Letters*, 287:453–462, 2009. doi:10.1016/j.epsl.2009.08.030.

[5] G. Baccolo, B. Delmonte, E. D. Stefano, G. Cibin, I. Crotti, M. Frezzotti, D. Hampai, Y. Iizuka, A. Marcelli, and V. Maggi. Deep ice as a geochemical reactor: Insights from iron speciation and mineralogy of dust in the Talos Dome ice core (East Antarctica). *Cryosphere*, 15:4807–4822, 2021. doi:10.5194/tc-15-4807-2021.

[6] C. M. Baglin. Nuclear Data Sheets for A = 81. *Nuclear Data Sheets*, 109:2257–2437, 2008. doi:10.1016/j.nds.2008.09.001.

[7] S. Baumgartner, J. Beer, M. Suter, B. Dittrich-Hannen, H.-A. Synal, P. W. Kubik, C. Hammer, and S. Johnsen. Chlorine 36 fallout in the Summit Greenland Ice Core Project ice core. *Journal of Geophysical Research: Oceans*, 102:26659–26662, 11 1997. doi:10.1029/97JC00166.

[8] S. Baumgartner, J. Beer, G. Wagner, P. Kubik, M. Suter, G. Raisbeck, and F. Yiou. 10Be and dust. *Nuclear Instruments and Methods in Physics Research Section B: Beam Interactions with Materials and Atoms*, 123: 296–301, 3 1997. doi:10.1016/S0168-583X(96)00751-3.

[9] S. Baumgartner, J. Beer, J. Masarik, G. Wagner, L. Meynadier, and H.-A. Synal. Geomagnetic Modulation of the 36Cl Flux in the GRIP Ice Core, Greenland. *Science*, 279:1330–1332, 2 1998. doi:10.1126/science.279.5355.1330.

[10] T. Bauska. *Ice core records of atmospheric carbon dioxide*, pages 122–137. Elsevier, 1 2025. ISBN 9780444536433. doi:10.1016/B978-0-323-99931-1.00264-6.

[11] J. Beer, K. McCracken, and R. von Steiger. *Cosmogenic Radionuclides*. Springer, 2019. ISBN 9781119130536.

[12] S. Benassai, S. Becagli, R. Gragnani, O. Magand, M. Proposito, I. Fattori, R. Traversi, and R. Udisti. Sea-spray deposition in Antarctic coastal and plateau areas from ITASE traverses. *Annals of Glaciology*, 41: 32–40, 9 2005. doi:10.3189/172756405781813285.

[13] M. L. Bender, B. Barnett, G. Dreyfus, J. Jouzel, and D. Porcelli. The contemporary degassing rate of 40Ar from the solid Earth. *Proceedings of the National Academy of Sciences of the United States of America*, 105: 8232–8237, 2008. doi:10.1073/pnas.0711679105.

[14] Beyond EPICA Consortium. Beyond EPICA Web Page, 9 2023. URL https://www.beyondepica.eu/en/.

[15] Beyond EPICA Consortium. Antarctica: Historic Drilling Campaign Reaches more than 1.2-Million-Year-Old Ice, 2025. URL https://www.beyondepica.eu/en/news-events/press-releases/.

[16] M. Bouchet, A. Landais, A. Grisart, F. Parrenin, F. Prié, R. Jacob, E. Fourré, E. Capron, D. Raynaud, V. Y. Lipenkov, M.-F. F. Loutre, T. Extier, A. Svensson, E. Legrain, P. Martinerie, M. Leuenberger, W. Jiang, F. Ritterbusch, Z.-T. T. Lu, and G.-M. M. Yang. The Antarctic Ice Core Chronology 2023 (AICC2023) chronological framework and associated timescale for the European Project for Ice Coring in Antarctica (EPICA) Dome C ice core. *Climate of the Past*, 19:2257–2286, 11 2023. doi:10.5194/cp-19-2257-2023.

[17] C. Buizert, D. Baggenstos, W. Jiang, R. Purtschert, V. V. Petrenko, Z. T. Lu, P. Müller, T. Kuhl, J. Lee, J. P. Severinghaus, and E. J. Brook. Radiometric 81Kr dating identifies 120,000-year-old ice at Taylor Glacier, Antarctica. *Proceedings of the National Academy of Sciences of the United States of America*, 111:6876–6881, 2014. doi:10.1073/pnas.1320329111.

[18] I. Büsching and M. S. Potgieter. The variability of the proton cosmic ray flux on the Sun's way around the galactic center. *Advances in Space Research*, 42:504–509, 2008. doi:10.1016/j.asr.2007.05.051.

[19] J. E. Channell, C. Xuan, and D. A. Hodell. Stacking paleointensity and oxygen isotope data for the last 1.5 Myr (PISO-1500). *Earth and Planetary Science Letters*, 283:14–23, 2009. doi:10.1016/j.epsl.2009.03.012.

[20] J. Chmeleff, F. von Blanckenburg, K. Kossert, and D. Jakob. Determination of the 10Be half-life by multicollector ICP-MS and liquid scintillation counting. *Nuclear Instruments and Methods in Physics Research Section B: Beam Interactions with Materials and Atoms*, 268:192–199, 1 2010. doi:10.1016/j.nimb.2009.09.012.

[21] M. Christl, C. Vockenhuber, P. W. Kubik, L. Wacker, J. Lachner, V. Alfimov, and H.-A. A. Synal. The ETH Zurich AMS facilities: Performance parameters and reference materials. *Nuclear Instruments and Methods in Physics Research, Section B: Beam Interactions with Materials and Atoms*, 294:29–38, 1 2013. doi:10.1016/j.nimb.2012.03.004.

[22] A. Cooper, C. S. M. Turney, J. Palmer, A. Hogg, M. McGlone, J. Wilmshurst, A. M. Lorrey, T. J. Heaton, J. M. Russell, K. McCracken, J. G. Anet, E. Rozanov, M. Friedel, I. Suter, T. Peter, R. Muscheler, F. Adolphi, A. Dosseto, J. T. Faith, P. Fenwick, C. J. Fogwill, K. Hughen, M. Lipson, J. Liu, N. Nowaczyk, E. Rainsley, C. B. Ramsey, P. Sebastianelli, Y. Souilmi, J. Stevenson, Z. Thomas, R. Tobler, and R. Zech. A global environmental crisis 42,000 years ago. *Science*, 371:811–818, 2 2021. doi:10.1126/science.abb8677.

[23] I. Crotti, A. Landais, B. Stenni, L. Bazin, F. Parrenin, M. Frezzotti, F. Ritterbusch, Z.-T. Lu, W. Jiang, G.-M. Yang, E. Fourré, A. Orsi, R. Jacob, B. Minster, F. Prié, G. Dreossi, and C. Barbante. An extension of the TALDICE ice core age scale reaching back to MIS 10.1. *Quaternary Science Reviews*, 266:107078, 8 2021. doi:10.1016/j.quascirev.2021.107078.

[24] D. Dahl-Jensen, M. R. Albert, A. Aldahan, N. Azuma, D. Balslev-Clausen, M. Baumgartner, A. M. Berggren, M. Bigler, T. Binder, T. Blunier, J. C. Bourgeois, E. J. Brook, S. L. Buchardt, C. Buizert, E. Capron, J. Chappellaz, J. Chung, H. B. Clausen, I. Cvijanovic, S. M. Davies, P. Ditlevsen, O. Eicher, H. Fischer, D. A. Fisher, L. G. Fleet, G. Gfeller, V. Gkinis, S. Gogineni, K. Goto-Azuma, A. Grinsted, H. Gudlaugsdottir, M. Guillevic, S. B. Hansen, M. Hansson, M. Hirabayashi, S. Hong, S. D. Hur, P. Huybrechts, C. S. Hvidberg, Y. Iizuka, T. Jenk, S. J. Johnsen, T. R. Jones, J. Jouzel, N. B. Karlsson, K. Kawamura, K. Keegan, E. Kettner, S. Kipfstuhl, H. A. Kjær, M. Koutnik, T. Kuramoto, P. Köhler, T. Laepple,

A. Landais, P. L. Langen, L. B. Larsen, D. Leuenberger, M. Leuenberger, C. Leuschen, J. Li, V. Lipenkov, P. Martinerie, O. J. Maselli, V. Masson-Delmotte, J. R. McConnell, H. Miller, O. Mini, A. Miyamoto, M. Montagnat-Rentier, R. Mulvaney, R. Muscheler, A. J. Orsi, J. Paden, C. Panton, F. Pattyn, J. R. Petit, K. Pol, T. Popp, G. Possnert, F. Prié, M. Prokopiou, A. Quiquet, S. O. Rasmussen, D. Raynaud, J. Ren, C. Reutenauer, C. Ritz, T. Röckmann, J. L. Rosen, M. Rubino, O. Rybak, D. Samyn, C. J. Sapart, A. Schilt, A. M. Schmidt, J. Schwander, S. Schüpbach, I. Seierstad, J. P. Severinghaus, S. Sheldon, S. B. Simonsen, J. Sjolte, A. M. Solgaard, T. Sowers, P. Sperlich, H. C. Steen-Larsen, K. Steffen, J. P. Steffensen, D. Steinhage, T. F. Stocker, C. Stowasser, A. S. Sturevik, W. T. Sturges, A. Sveinbjörnsdottir, A. Svensson, J. L. Tison, J. Uetake, P. Vallelonga, R. S. V. D. Wal, G. V. D. Wel, B. H. Vaughn, B. Vinther, E. Waddington, A. Wegner, I. Weikusat, J. W. White, F. Wilhelms, M. Winstrup, E. Witrant, E. W. Wolff, C. Xiao, and J. Zheng. Eemian interglacial reconstructed from a Greenland folded ice core. *Nature*, 493:489–494, 2013. doi:10.1038/nature11789.

[25] M. de Angelis, J. L. Tison, M. C. Morel-Fourcade, and J. Susini. Micro-investigation of EPICA Dome C bottom ice: Evidence of long term in situ processes involving acid-salt interactions, mineral dust, and organic matter. *Quaternary Science Reviews*, 78:248–265, 2013. doi:10.1016/j.quascirev.2013.08.012.

[26] R. J. Delmas, J. Beer, H. A. A. Synal, R. Muscheler, J. R. R. Petit, and M. Pourchet. Bomb-test 36Cl measurements in Vostok snow (Antarctica) and the use of 36Cl as a dating tool for deep ice cores. *Tellus, Series B: Chemical and Physical Meteorology*, 56:492–498, 1 2004. doi:10.1111/j.1600-0889.2004.00109.x.

[27] K. Diehl, S. Mitra, and H. Pruppacher. A laboratory study of the uptake of HNO3 and HCl vapor by snow crystals and ice spheres at temperatures between 0 and –40°C. *Atmospheric Environment*, 29:975–981, 5 1995. doi:10.1016/1352-2310(95)00022-Q.

[28] A. A. Ekaykin, V. Y. Lipenkov, N. I. Barkov, J. R. Petit, and V. Masson-Delmotte. Spatial and temporal variability in isotope composition of recent snow in the vicinity of Vostok station, Antarctica: implications for ice-core record interpretation. *Annals of Glaciology*, 35:181–186, 9 2002. doi:10.3189/172756402781816726.

[29] D. Elmore, L. E. Tubbs, D. Newman, X. Z. Ma, R. Finkel, K. Nishiizumi, J. Beer, H. Oeschger, and M. Andree. 36Cl bomb pulse measured in a shallow ice core from Dye 3, Greenland. *Nature*, 300: 735–737, 12 1982. doi:10.1038/300735a0.

[30] D. Elmore, N. J. Conard, P. W. Kubik, H. E. Gove, M. Wahlen, J. Beer, and M. Suter. 36Cl and 10Be profiles in greenland ice: Dating and production rate variations. *Nuclear Instruments and Methods in Physics Research Section B: Beam Interactions with Materials and Atoms*, 29:207–210, 11 1987. doi:10.1016/0168-583X(87)90237-0.

[31] P. Endt and C. van dèr Leun. Energy levels of A = 21–44 nuclei (V). *Nuclear Physics A*, 214:1–625, 10 1973. doi:10.1016/0375-9474(73)91131-7.

[32] C. V. Field, G. A. Schmidt, D. Koch, and C. Salyk. Modeling production and climate-related impacts on 10Be concentration in ice cores. *Journal of Geophysical Research Atmospheres*, 111:1–13, 2006. doi:10.1029/2005JD006410.

[33] A. Fuchs and M. C. Leuenberger. δ18O of atmospheric oxygen measured on the GRIP Ice Core Document Stratigraphic disturbances in the lowest 10% of the core. *Geophysical Research Letters*, 23:1049–1052, 5 1996. doi:10.1029/96GL00588.

[34] H. Fukazawa, K. Sugiyama, S. Mae, H. Narita, and T. Hondoh. Acid ions at triple junction of Antarctic ice observed by Raman scattering. *Geophysical Research Letters*, 25:2845–2848, 1998. doi:10.1029/98GL02178.

[35] L. Gerrish, L. Ireland, P. Fretwell, and P. Cooper. Medium resolution vector polygons of the Antarctic coastline (Version 7.10), 11 2024. doi:10.5285/58f290ec-b729-40fa-95de-2fa1ac1ba265.

[36] L. J. Gleeson and W. I. Axford. Solar Modulation of Galactic Cosmic Rays. *The Astrophysical Journal*, 154: 1011, 12 1968. doi:10.1086/149822.

[37] P. M. Grootes, M. Stuiver, J. W. C. White, S. Johnsen, and J. Jouzel. Comparison of oxygen isotope records from the GISP2 and GRIP Greenland ice cores. *Nature*, 366:552–554, 12 1993. doi:10.1038/366552a0.

[38] U. Heikkilä and A. M. Smith. Production rate and climate influences on the variability of 10Be deposition simulated by ECHAM5 HAM: Globally, in Greenland, and in Antarctica. *Journal of Geophysical Research: Atmospheres*, 118:2506–2520, 3 2013. doi:10.1002/jgrd.50217.

[39] U. Heikkilä, J. Beer, and J. Feichter. Modeling cosmogenic radionuclides 10Be and 7Be during the maunder minimum using the ECHAM5-HAM general circulation Model. *Atmospheric Chemistry and Physics*, 8:2797–2809, 2008. doi:10.5194/acp-8-2797-2008.

[40] U. Heikkilä, J. Beer, and J. Feichter. Meridional transport and deposition of atmospheric 10Be. *Atmospheric Chemistry and Physics*, 9:515–527, 2009. doi:10.5194/acp-9-515-2009.

[41] U. Heikkilä, J. Beer, J. Feichter, V. Alfimov, H.-A. Synal, U. Schotterer, A. Eichler, M. Schwikowski, and L. Thompson. 36Cl bomb peak: comparison of modeled and measured data. *Atmospheric Chemistry and Physics*, 9:4145–4156, 6 2009. doi:10.5194/acp-9-4145-2009.

[42] U. Heikkilä, J. Beer, J. A. Abreu, and F. Steinhilber. On the Atmospheric Transport and Deposition of the Cosmogenic Radionuclides (10Be): A Review. *Space Science Reviews*, 176:321–332, 6 2013. doi:10.1007/s11214-011-9838-0.

[43] K. Herbst, R. Muscheler, and B. Heber. The new local interstellar spectra and their influence on the production rates of the cosmogenic radionuclides 10Be and 14C. *Journal of Geophysical Research: Space Physics*, 122:23–34, 1 2017. doi:10.1002/2016JA023207.

[44] H. M. Hoffmann, M. M. Grieman, A. C. King, J. A. Epifanio, K. Martin, D. Vladimirova, H. V. Pryer, E. Doyle, A. Schmidt, J. D. Humby, I. F. Rowell, C. Nehrbass-Ahles, E. R. Thomas, R. Mulvaney, and E. W. Wolff. The ST22 chronology for the Skytrain Ice Rise ice core - Part 1: A stratigraphic chronology of the last 2000 years. *Climate of the Past*, 18:1831–1847, 2022. doi:10.5194/cp-18-1831-2022.

[45] B. Jourdain and M. Legrand. Year-round records of bulk and size-segregated aerosol composition and HCl and HNO3 levels in the Dumont d'Urville (coastal Antarctica) atmosphere: Implications for sea-salt aerosol fractionation in the winter and summer. *Journal of Geophysical Research: Atmospheres*, 107:4645, 11 2002. doi:10.1029/2002JD002471.

[46] J. Jouzel, V. Masson-Delmotte, O. Cattani, G. Dreyfus, S. Falourd, G. Hoffmann, B. Minster, J. Nouet, J. M. Barnola, J. Chappellaz, H. Fischer, J. C. Gallet, S. Johnsen, M. Leuenberger, L. Loulergue, D. Luethi, H. Oerter, F. Parrenin, G. Raisbeck, D. Raynaud, A. Schilt, J. Schwander, E. Selmo, R. Souchez, R. Spahni, B. Stauffer, J. P. Steffensen, B. Stenni, T. F. Stocker, J. L. Tison, M. Werner, and E. W. Wolff. Orbital and Millennial Antarctic Climate Variability over the Past 800,000 Years. *Science*, 317:793–796, 8 2007. doi:10.1126/science.1141038.

[47] K. Kanzawa, F. Miyake, K. Horiuchi, K. Sasa, K. Takano, M. Matsumura, T. Takahashi, Y. Motizuki, K. Takahashi, Y. Nakai, K. Ohtani, Y. Tada, Y. Ochiai, H. Motoyama, H. Matsuzaki, A. Yamazaki, Y. Muramatsu, and T. Yamagata. High-Resolution 10 Be and 36 Cl Data From the Antarctic Dome Fuji Ice Core (100 Years Around 5480 BCE): An Unusual Grand Solar Minimum Occurrence? *Journal of Geophysical Research: Space Physics*, 126, 10 2021. doi:10.1029/2021JA029378.

[48] N. Kappelt, R. Muscheler, M. Baroni, J. Beer, M. Christl, C. Vockenhuber, E. Bard, and E. Wolff. Ice core dating with the 36Cl/10Be ratio. *Quaternary Science Reviews*, 355:109254, 5 2025. doi:10.1016/j.quascirev.2025.109254.

[49] M. D. Keywood, L. K. Fifield, A. R. Chivas, and R. G. Cresswell. Fallout of chlorine 36 to the Earth's surface in the Southern Hemisphere. *Journal of Geophysical Research Atmospheres*, 103:8281–8286, 4 1998. doi:10.1029/97JD03125.

[50] S. Kipfstuhl, I. Hamann, A. Lambrecht, J. Freitag, S. H. Faria, D. Grigoriev, and N. Azuma. Microstructure mapping: A new method for imaging deformation-induced microstructural features of ice on the grain scale. *Journal of Glaciology*, 52:398–406, 2006. doi:10.3189/172756506781828647.

[51] D. L. Knies, D. Elmore, P. Sharma, S. Vogt, R. Li, M. E. Lipschutz, G. Petty, J. Farrell, M. C. Monaghan, S. Fritz, and E. Agee. 7Be, 10Be, and 36Cl in precipitation. *Nuclear Inst. and Methods in Physics Research, B*, 92:340–344, 1994. doi:10.1016/0168-583X(94)96031-3.

[52] G. Korschinek, A. Bergmaier, T. Faestermann, U. Gerstmann, K. Knie, G. Rugel, A. Wallner, I. Dillmann, G. Dollinger, C. L. von Gostomski, K. Kossert, M. Maiti, M. Poutivtsev, and A. Remmert. A new value for the half-life of 10Be by Heavy-Ion Elastic Recoil Detection and liquid scintillation counting. *Nuclear Instruments and Methods in Physics Research Section B: Beam Interactions with Materials and Atoms*, 268: 187–191, 1 2010. doi:10.1016/j.nimb.2009.09.020.

[53] M. Legrand, S. Preunkert, E. Wolff, R. Weller, B. Jourdain, and D. Wagenbach. Year-round records of bulk and size-segregated aerosol composition in central Antarctica (Concordia site) - Part 1: Fractionation of sea-salt particles. *Atmospheric Chemistry and Physics*, 17:14039–14054, 11 2017. doi:10.5194/acp-17-14039-2017.

[54] M. R. Legrand and R. J. Delmas. Formation of HCl in the Antarctic atmosphere. *Journal of Geophysical Research: Atmospheres*, 93:7153–7168, 6 1988. doi:10.1029/JD093iD06p07153.

[55] H. Loosli and H. Oeschger. 37Ar and 81Kr in the atmosphere. *Earth and Planetary Science Letters*, 7: 67–71, 10 1969. doi:10.1016/0012-821X(69)90014-4.

[56] C. E. Lukasczyk. *36Chlor in Grönlandeis*. PhD thesis, ETH Zürich, 1994. doi:10.3929/ethz-a-000965554.

[57] J. Lyman and R. H. Fleming. Composition of Seawater. *Journal of Marine Research*, 3:134–146, 1940. URL https://elischolar.library.yale.edu/journal_of_marine_research/566.

[58] R. Mulvaney, K. Oates, and E. W. Wolff. Sulphuric acid at grain boundaries in Antarctic ice. *Nature*, 331: 247–249, 1988. doi:10.1038/331247a0.

[59] R. Mulvaney, J. Rix, S. Polfrey, M. Grieman, C. Martìn, C. Nehrbass-Ahles, I. Rowell, R. Tuckwell, and E. Wolff. Ice drilling on Skytrain Ice Rise and Sherman Island, Antarctica. *Annals of Glaciology*, 62: 311–323, 9 2021. doi:10.1017/aog.2021.7.

[60] R. Mulvaney, E. W. Wolff, M. M. Grieman, H. H. Hoffmann, J. D. Humby, C. Nehrbass-Ahles, R. H. Rhodes, I. F. Rowell, F. Parrenin, L. Schmidely, H. Fischer, T. F. Stocker, M. Christl, R. Muscheler, A. Landais, and F. Prié. The ST22 chronology for the Skytrain Ice Rise ice core – Part 2: An age model to the last interglacial and disturbed deep stratigraphy. *Climate of the Past*, 19:851–864, 4 2023. doi:10.5194/cp-19-851-2023.

[61] R. Muscheler. *Nachweis von Änderungen im Kohlenstoffkreislauf durch Vergleich der Radionuklide 10Be, 36Cl und 14C*. PhD thesis, ETH Zürich, 2000. doi:10.3929/ethz-a-004179578.

[62] R. Muscheler, J. Beer, P. W. Kubik, and H. A. Synal. Geomagnetic field intensity during the last 60,000 years based on 10Be and 36Cl from the Summit ice cores and 14C. *Quaternary Science Reviews*, 24:1849–1860, 2005. doi:10.1016/j.quascirev.2005.01.012.

[63] R. Muscheler, F. Adolphi, K. Herbst, and A. Nilsson. The Revised Sunspot Record in Comparison to Cosmogenic Radionuclide-Based Solar Activity Reconstructions. *Solar Physics*, 291:3025–3043, 2016. doi:10.1007/s11207-016-0969-z.

[64] A. Nilsson, L. Nguyen, S. Panovska, K. Herbst, M. Zheng, N. Suttie, and R. Muscheler. Holocene solar activity inferred from global and hemispherical cosmic-ray proxy records. *Nature Geoscience*, 17:654–659, 7 2024. doi:10.1038/s41561-024-01467-5.

[65] K. Nishiizumi, J. Arnold, D. Elmore, X. Ma, D. Newman, and H. Gove. 36Cl and 53Mn in Antarctic meteorites and 10Be/36Cl dating of Antarctic ice. *Earth and Planetary Science Letters*, 62:407–417, 3 1983. doi:10.1016/0012-821X(83)90011-0.

[66] K. Nishiizumi, M. Imamura, M. W. Caffee, J. R. Southon, R. C. Finkel, and J. McAninch. Absolute calibration of 10Be AMS standards. *Nuclear Instruments and Methods in Physics Research, Section B: Beam Interactions with Materials and Atoms*, 258:403–413, 2007. doi:10.1016/j.nimb.2007.01.297.

[67] J. Pedro, J. McConnell, T. van Ommen, D. Fink, M. Curran, A. Smith, K. Simon, A. Moy, and S. Das. Solar and climate influences on ice core 10Be records from Antarctica and Greenland during the neutron monitor era. *Earth and Planetary Science Letters*, 355-356:174–186, 11 2012. doi:10.1016/j.epsl.2012.08.038.

[68] J. B. Pedro, U. E. Heikkilä, A. Klekociuk, A. M. Smith, T. D. V. Ommen, and M. A. Curran. Beryllium-10 transport to Antarctica: Results from seasonally resolved observations and modeling. *Journal of Geophysical Research Atmospheres*, 116:1–14, 2011. doi:10.1029/2011JD016530.

[69] S. Pivot, M. Baroni, E. Bard, and X. Giraud. A Comparison of 36Cl Nuclear Bomb Inputs Deposited in Snow From Vostok and Talos Dome, Antarctica, Using the 36Cl/Cl– ratio. *Journal of Geophysical Research: Atmospheres*, 124:10973–10988, 2019. doi:10.1029/2018JD030200.

[70] S. Poluianov, G. A. Kovaltsov, A. L. Mishev, and I. G. Usoskin. Production of Cosmogenic Isotopes 7Be, 10Be, 14C, 22Na, and 36Cl in the Atmosphere: Altitudinal Profiles of Yield Functions. *Journal of Geophysical Research: Atmospheres*, 121:8125–8136, 6 2016. doi:10.1002/2016JD025034.

[71] G. Raisbeck and F. Yiou. 10Be in Polar Ice and Atmospheres. *Annals of Glaciology*, 7:138–140, 1985. doi:10.3189/s0260305500006054.

[72] G. M. Raisbeck, F. Yiou, M. Fruneau, J. M. Loiseaux, M. Lieuvin, and J. C. Ravel. Cosmogenic 10Be/7Be as a probe of atmospheric transport processes. *Geophysical Research Letters*, 8:1015–1018, 9 1981. doi:10.1029/GL008i009p01015.

[73] G. M. Raisbeck, F. Yiou, O. Cattani, and J. Jouzel. 10Be evidence for the Matuyama–Brunhes geomagnetic reversal in the EPICA Dome C ice core. *Nature*, 444:82–84, 11 2006. doi:10.1038/nature05266.

[74] A. M. Rankin, E. W. Wolff, and R. Mulvaney. A reinterpretation of sea-salt records in Greenland and Antarctic ice cores? *Annals of Glaciology*, 39:276–282, 2004. doi:10.3189/172756404781814681.

[75] A. W. Rempel, J. S. Wettlaufer, and E. D. Waddington. Anomalous diffusion of multiple impurity species: Predicted implications for the ice core climate records. *Journal of Geophysical Research: Solid Earth*, 107, 12 2002. doi:10.1029/2002jb001857.

[76] F. Ritterbusch, J. S. Wang, X. Feng, S. Shackleton, M. Bender, E. Brook, J. Higgins, Z.-H. Jia, W. Jiang, Z.-T. Lu, J. P. Severinghaus, L.-T. Sun, G.-M. Yang, and L. Zhao. 81Kr dating of 1 kg Antarctic ice. *Nature Communications*, 16:4394, 5 2025. doi:10.1038/s41467-025-59264-6.

[77] J. Rix, R. Mulvaney, J. Hong, and D. Ashurst. Development of the British Antarctic Survey Rapid Access Isotope Drill. *Journal of Glaciology*, 65:288–298, 4 2019. doi:10.1017/jog.2019.9.

[78] I. F. Rowell. *New ice core records from West Antarctica and their spatial context: from 1000 to 100,000 years*. PhD thesis, University of Cambridge, 2022. doi:10.17863/CAM.94392.

[79] I. F. Rowell, R. Mulvaney, J. Rix, D. R. Tetzner, and E. W. Wolff. Viability of chemical and water isotope ratio measurements of RAID ice chippings from Antarctica. *Journal of Glaciology*, 69:623–638, 6 2023. doi:10.1017/jog.2022.94.

[80] U. Ruth, J.-M. Barnola, J. Beer, M. Bigler, T. Blunier, E. Castellano, H. Fischer, F. Fundel, P. Huybrechts, P. Kaufmann, S. Kipfstuhl, A. Lambrecht, A. Morganti, H. Oerter, F. Parrenin, O. Rybak, M. Severi, R. Udisti, F. Wilhelms, and E. Wolff. "EDML1": a chronology for the EPICA deep ice core from Dronning Maud Land, Antarctica, over the last 150 000 years. *Climate of the Past*, 3:475–484, 8 2007. doi:10.5194/cp-3-475-2007.

[81] R. Röthlisberger, R. Mulvaney, E. W. Wolff, M. A. Hutterli, M. Bigler, M. de Angelis, M. E. Hansson, J. P. Steffensen, and R. Udisti. Limited dechlorination of sea-salt aerosols during the last glacial period: Evidence from the European Project for Ice Coring in Antarctica (EPICA) Dome C ice core. *Journal of Geophysical Research: Atmospheres*, 108:1–6, 2003. doi:10.1029/2003jd003604.

[82] T. Sakurai, H. Ohno, H. Motoyama, and T. Uchida. Micro-droplets containing sulfate in the Dome Fuji deep ice core, Antarctica: findings using micro-Raman spectroscopy. *Journal of Raman Spectroscopy*, 48: 448–452, 2017. doi:10.1002/jrs.5040.

[83] J. Schwander, J. Jouzel, C. U. Hammer, J.-R. Petit, R. Udisti, and E. Wolff. A tentative chronology for the EPICA Dome Concordia Ice Core. *Geophysical Research Letters*, 28:4243–4246, 11 2001. doi:10.1029/2000GL011981.

[84] L. C. Slivinski, G. P. Compo, P. D. Sardeshmukh, J. S. Whitaker, C. McColl, R. J. Allan, P. Brohan, X. Yin, C. A. Smith, L. J. Spencer, R. S. Vose, M. Rohrer, R. P. Conroy, D. C. Schuster, J. J. Kennedy, L. Ashcroft, S. Brönnimann, M. Brunet, D. Camuffo, R. Cornes, T. A. Cram, F. Domínguez-Castro, J. E. Freeman, J. Gergis, E. Hawkins, P. D. Jones, H. Kubota, T. C. Lee, A. M. Lorrey, J. Luterbacher, C. J. Mock, R. K. Przybylak, C. Pudmenzky, V. C. Slonosky, B. Tinz, B. Trewin, X. L. Wang, C. Wilkinson, K. Wood, and P. Wyszynski. An evaluation of the performance of the twentieth century reanalysis version 3. *Journal of Climate*, 34:1417–1438, 2021. doi:10.1175/JCLI-D-20-0505.1.

[85] F. Steinhilber, J. A. Abreu, J. Beer, I. Brunner, M. Christl, H. Fischer, U. Heikkilä, P. W. Kubik, M. Mann, K. G. McCracken, H. Miller, H. Miyahara, H. Oerter, and F. Wilhelms. 9,400 years of cosmic radiation and solar activity from ice cores and tree rings. *Proceedings of the National Academy of Sciences*, 109:5967–5971, 4 2012. doi:10.1073/pnas.1118965109.

[86] P. Stier, J. Feichter, S. Kinne, S. Kloster, E. Vignati, J. Wilson, L. Ganzeveld, I. Tegen, M. Werner, Y. Balkanski, M. Schulz, O. Boucher, A. Minikin, and A. Petzold. The aerosol-climate model ECHAM5-HAM. *Atmospheric Chemistry and Physics*, 5:1125–1156, 3 2005. doi:10.5194/acp-5-1125-2005.

[87] A. L. Stuart and M. Z. Jacobson. A timescale investigation of volatile chemical retention during hydrometeor freezing: Nonrime freezing and dry growth riming without spreading. *Journal of Geophysical Research: Atmospheres*, 108:1–16, 3 2003. doi:10.1029/2001JD001408.

[88] H.-A. Synal, J. Beer, G. Bonani, M. Suter, and W. Wölfli. Atmospheric transport of bomb-produced 36Cl. *Nuclear Instruments and Methods in Physics Research Section B: Beam Interactions with Materials and Atoms*, 52:483–488, 12 1990. doi:10.1016/0168-583X(90)90462-4.

[89] J. L. Tison, M. D. Angelis, G. Littot, E. Wolff, H. Fischer, M. Hansson, M. Bigler, R. Udisti, A. Wegner, J. Jouzel, B. Stenni, S. Johnsen, V. Masson-Delmotte, A. Landais, V. Lipenkov, L. Loulergue, J. M. Barnola, J. R. Petit, B. Delmonte, G. Dreyfus, D. Dahl-Jensen, G. Durand, B. Bereiter, A. Schilt, R. Spahni, K. Pol, R. Lorrain, R. Souchez, and D. Samyn. Retrieving the paleoclimatic signal from the deeper part of the EPICA Dome C ice core. *Cryosphere*, 9:1633–1648, 8 2015. doi:10.5194/tc-9-1633-2015.

[90] I. G. Usoskin, A. Gil, G. A. Kovaltsov, A. L. Mishev, and V. V. Mikhailov. Heliospheric modulation of cosmic rays during the neutron monitor era: Calibration using PAMELA data for 2006–2010. *Journal of Geophysical Research: Space Physics*, 122:3875–3887, 4 2017. doi:10.1002/2016JA023819.

[91] D. Voisin, M. Legrand, and N. Chaumerliac. Scavenging of acidic gases (HCOOH, CH3COOH, HNO3 , HCl, and SO2) and ammonia in mixed liquid-solid water clouds at the Puy de Dôme mountain (France). *Journal of Geophysical Research: Atmospheres*, 105:6817–6835, 3 2000. doi:10.1029/1999JD900983.

[92] G. Wagner. *Die kosmogenen Radionuklide 10Be und 36Cl im Summit-GRIP-Eisbohrkern.* PhD thesis, ETH Zürich, 1998. doi:10.3929/ethz-a-002074084.

[93] G. Wagner, J. Masarik, J. Beer, S. Baumgartner, D. Imboden, P. W. Kubik, H. A. Synal, and M. Suter. Reconstruction of the geomagnetic field between 20 and 60 kyr BP from cosmogenic radionuclides in the GRIP ice core. *Nuclear Instruments and Methods in Physics Research, Section B: Beam Interactions with Materials and Atoms*, 172:597–604, 2000. doi:10.1016/S0168-583X(00)00285-8.

[94] G. Wagner, J. Beer, J. Masarik, R. Muscheler, P. W. Kubik, W. Mende, C. Laj, G. M. Raisbeck, and F. Yiou. Presence of the solar de Vries cycle (~205 years) during the last ice age. *Geophysical Research Letters*, 28: 303–306, 1 2001. doi:10.1029/2000GL006116.

[95] P. Wagnon, R. J. Delmas, and M. Legrand. Loss of volatile acid species from upper firn layers at Vostok, Antarctica. *Journal of Geophysical Research Atmospheres*, 104:3423–3431, 2 1999. doi:10.1029/98JD02855.

[96] E. Wolff, X. Feng, W. Jiang, Z.-T. Lu, F. Ritterbusch, J. Wang, G.-M. Yang, A. Landais, E. Fourré, T. Combacal, N. Kappelt, R. Muscheler, and R. Mulvaney. Ice half a million years old at the base of the Skytrain Ice Rise ice core. In *EGU 2025*. EGU, 3 2025. doi:10.5194/egusphere-egu25-6428.

[97] E. W. Wolff, C. Barbante, S. Becagli, M. Bigler, C. F. Boutron, E. Castellano, M. de Angelis, U. Federer, H. Fischer, F. Fundel, M. Hansson, M. Hutterli, U. Jonsell, T. Karlin, P. Kaufmann, F. Lambert, G. C. Littot, R. Mulvaney, R. Röthlisberger, U. Ruth, M. Severi, M. L. Siggaard-Andersen, L. C. Sime, J. P. Steffensen, T. F. Stocker, R. Traversi, B. Twarloh, R. Udisti, D. Wagenbach, and A. Wegner. Changes in environment over the last 800,000 years from chemical analysis of the EPICA Dome C ice core. *Quaternary Science Reviews*, 29:285–295, 2010. doi:10.1016/j.quascirev.2009.06.013.

[98] E. W. Wolff, R. Mulvaney, M. M. Grieman, H. M. Hoffmann, J. Humby, C. Nehrbass-Ahles, R. H. Rhodes, I. F. Rowell, L. C. Sime, H. Fischer, T. F. Stocker, A. Landais, F. Parrenin, E. J. Steig, M. Dütsch, and N. R. Golledge. The Ronne Ice Shelf survived the last interglacial. *Nature*, 638:133–137, 2 2025. doi:10.1038/s41586-024-08394-w.

[99] Y. Yan, M. L. Bender, E. J. Brook, H. M. Clifford, P. C. Kemeny, A. V. Kurbatov, S. Mackay, P. A. Mayewski, J. Ng, J. P. Severinghaus, and J. A. Higgins. Two-million-year-old snapshots of atmospheric gases from Antarctic ice. *Nature*, 574:663–666, 2019. doi:10.1038/s41586-019-1692-3.

[100] A. M. Yau, M. L. Bender, T. Blunier, and J. Jouzel. Setting a chronology for the basal ice at Dye-3 and GRIP: Implications for the long-term stability of the Greenland Ice Sheet. *Earth and Planetary Science Letters*, 451:1–9, 10 2016. doi:10.1016/j.epsl.2016.06.053.

[101] F. Yiou, G. M. Raisbeck, S. Baumgartner, J. Beer, C. Hammer, S. Johnsen, J. Jouzel, P. W. Kubik, J. Lestringuez, M. Stiévenard, M. Suter, and P. Yiou. Beryllium 10 in the Greenland Ice Core Project ice core at Summit, Greenland. *Journal of Geophysical Research: Oceans*, 102:26783–26794, 11 1997. doi:10.1029/97JC01265.

[102] J. C. Zappala, D. Baggenstos, C. Gerber, W. Jiang, B. M. Kennedy, Z. T. Lu, J. Masarik, P. Mueller, R. Purtschert, and A. Visser. Atmospheric 81Kr as an Integrator of Cosmic-Ray Flux on the Hundred-Thousand-Year Time Scale. *Geophysical Research Letters*, 47:1–7, 2020. doi:10.1029/2019GL086381.

[103] L. Zerle, T. Faestermann, K. Knie, G. Korschinek, E. Nolte, J. Beer, and U. Schotterer. The 41Ca bomb pulse and atmospheric transport of radionuclides. *Journal of Geophysical Research Atmospheres*, 102:19517–19527, 1997. doi:10.1029/97jd00701.

[104] M. Zheng, A. Sturevik-Storm, A. Nilsson, F. Adolphi, A. Aldahan, G. Possnert, and R. Muscheler. Geomagnetic dipole moment variations for the last glacial period inferred from cosmogenic radionuclides in Greenland ice cores via disentangling the climate and production signals. *Quaternary Science Reviews*, 258, 2021. doi:10.1016/j.quascirev.2021.106881.

[105] M. Zheng, R. Muscheler, F. Adolphi, F. Mekhaldi, Z. Lu, M. Wu, A. Synal, J. Beer, and U. Lohmann. Atmospheric transport and deposition of cosmogenic 36Cl using ECHAM6.3-HAM2.3 model. *Earth and Planetary Science Letters*, 666:119494, 9 2025. doi:10.1016/j.epsl.2025.119494.

Scientific publications

LUNDQUA Publications

At the Department of Geology, Quaternary Sciences, Lund University, three series are published, named "Thesis", "Report" and "Uppdrag". The "Thesis" series contains doctor dissertations; the "Report" series primary material, often of a monographic character, which cannot be published in extenso in ordinary scientific journals; the "Uppdrag" series contains selected examples of expert reports, generally in Swedish, which may be of some general interest.

The "Thesis" and the "Report" series cover different aspects of Quaternary stratigraphy and environment—methods, lithostratigraphy, biostratigraphy, chronology, as well as their applications within technical geology, resource geology, nature conservancy, archaeology etc. Complete lists of publications may be ordered from the Department of Geology, Quaternary Sciences, Sölvegatan 12, SE-223 62 Lund, Sweden.

1. Nilsson, K. 1973: Glacialgeologiska problem i Sydvästskåne (English summary: Problems of glacial geology in south-western Scania).

2. Bjelm, L. 1976: Deglaciationen av Småländska höglandet, speciellt med avseende på deglaciationsdynamik, ismäktighet och tidsställning. (Deglaciation of the Småland Highland, with special reference to deglaciation dynamics, ice thickness and chronology).

3. Göransson, H. 1977: The Flandrian Vegetational History of Southern Östergötland.

4. Miller, U. 1977: Pleistocene deposits of the Alnarp Valley, southern Sweden Microfossils and their stratigraphic application.

5. Lagerlund, E. 1977: Förutsättningar för moränstratigrafiska undersökningar på Kullen i Nordvästskåne—teoriutveckling och neotektonik (Till stratigraphical studies in the Kullen area, NW Skåne, South Sweden: basic theory and neotectonics).

6. Hilldén, A. 1979: Deglaciationsförloppet i trakten av Berghemsmoränen, öster om Göteborg (English summary: The deglaciation in the vicinity of the Berghem moraine, east of Göteborg).

7. Björck, S. 1979: Late Weichselian stratigraphy of Blekinge, SE Sweden, and water level changes in the Baltic Ice Lake.

8. Andersson, O.H. 1981: Borrning och dokumentation. Borrningsteknik jämte metodik för geologisk datainsamling under borrningsgång (Drilling and documentation).

9. Hjort, C. 1981: Studies of the Quaternary in Northeast Greenland.

10. Hjelmroos Ericson, M. 1981: Holocene development of Lake Wielkie Gacno area, northwestern Poland.

11. Liljegren, R. 1982: Paleoekologi och strandförskjutning i en Littorinavik vid Spjälkö i mellersta Blekinge (English summary: Palaeoecology and shore displacement in a Littorina bay at Spjälkö, Blekinge).

12. Norddahl, H. 1983: Late Quaternary stratigraphy of Fnjóskadalur central North Iceland, a study of sediments, ice lake strandlines, glacial isostasy and ice free areas.

13. Robison, J.M. 1983: Glaciofluvial sedimentation: A key to the deglaciation of the Laholm area, southern Sweden.

14. Sandgren, P. 1983: The deglaciation of the Klippan area, southern Sweden, a study of glaciofluvial and glaciomarine sediments.

15. Åmark, M. 1984: The deglaciation of the eastern part of Skåne, southern Sweden. A study of till and stratified drift.

16. Adrielsson, L. 1984: Weichselian lithostratigraphy and glacial environments in the Ven Glumslöv area, southern Sweden.

17. Waldemarson, D. 1986: Weichselian lithostratigraphy, depositional processes and deglaciation pattern in the southern Vättern basin, south Sweden.

18. Hallsdottir, M. 1987: Pollen analytical studies of human influence on vegetation in relation to the Landnam tephra layer in southwest Iceland.

19. Ingolfsson, O. 1987: Investigation of the Late Weichselian glacial history of the lower Borgarfjördur region, western Iceland.

20. Möller, P. 1987: Moraine morphology, till genesis, and deglaciation pattern in the Åsnen area, south central Småland, Sweden.

21. Harrison, S. 1988: Reconstructing climate from lake level changes.

22. Lemdahl, G. 1988: Palaeoclimatic and palaeoecological studies based on subfossil insects from Late Weichselian sediments in southern Sweden.

23. Malmberg Persson, K. 1988: Lithostratigraphic and sedimentological investigations around the eastern boundary of the Baltic deposits in central Scania.

24. Liedberg Jönsson, B. 1988: The Late Weichselian macrofossil flora in western Skåne, southern Sweden.

25. Svensson, N.O. 1989: Late Weichselian and early Holocene shore displacement in the central Baltic, based on stratigraphical and morphological records from eastern Småland and Gotland, Sweden.

26. Thelaus, M. 1989: Late Quaternary vegetation history and palaeohydrology of the Sandsjön-Årshult area, southwestern Sweden

27. Regnéll, J. 1989: Vegetation and land use during 6000 years. Palaeoecology of the cultural landscape at two lake sites in southern Skåne, Sweden.

28. Olsson, S. 1991: Geochemistry, mineralogy and pore water composition in uplifted, Late Weichselian -Early Holocene clays from southern Sweden.

29. Ekström, J. 1993: The Late Quaternary History of the Urus (Bos primigenius Bojanus 1827) in Sweden.

30. Almquist Jacobson, H. 1994: Interaction of the Holocene climate, water balance, vegetation, fire, and the cultural land use in the Swedish Borderland.

31. Hammarlund, D. 1994: Stable carbon and oxygen isotope studies of Late Weichselian lake sediments in southern Sweden and northern Poland, with palaeoclimatic implications.

32. Eggertsson, Ò. 1994: Origin of the Arctic driftwood a dendrochronological study.

33. Sæmundsson, T. 1995: Deglaciation and shoreline displacement in Vopnafjördur, northeastern Iceland.

34. Snowball, I.F. 1995: Mineral magnetic and geochemical properties of Holocene sediments and soils in the Abisko region of northern Sweden.

35. Berglund, M. 1995: The Late Weichselian deglaciation, vegetational development and shore displacement in Halland, southwestern Sweden.

36. Lagerås, P. 1996: Vegetation and land use in the Småland Uplands, southern Sweden, during the last 6000 years.

37. Yu, G. 1996: Lake level records and palaeoclimates of northern Eurasia.

38. Jiang, H. 1996: Palaeoclimate and palaeoceanography of the Skagerrak-Kattegat since the Late Weichselian based on diatom records.

39. Björkman, L. 1996: The Late Holocene history of beech Fagus sylvatica and Norway spruce Picea abies at stand scale in southern Sweden.

40. Rundgren, M. 1997: Late Weichselian and early Holocene changes of vegetation, climate and sea level on the Skagi peninsula, northern Iceland.

41. Vassiljev, J. 1997: Simulating the paleorecord of northern European lakes using a coupled lake catchment model.

42. Andersson, G. 1997: Deglaciation pattern and dynamics in the Bolmen area, southwestern Sweden.

43. Barnekow, L. 1999: Holocene vegetation dynamics and climate changes in the Torneträsk area, northern Sweden.

44. Ising, J. 2001: Pollen analysis, chronology and palaeomagnetism of three Late Weichselian sites in southern Sweden.

45. Gedda, B. 2001: Environmental and climatic aspects of the early to mid Holocene calcareous tufa and land mollusc fauna in southern Sweden.

46. Broström, A. 2002: Estimating source area of pollen and pollen productivity in the cultural landscapes of southern Sweden—developing a palynological tool for quantifying past plant cover.

47. Pettersson, G. 2002: Weichselian glaciations in the middle Notec River region, northwest Poland.

48. Alexanderson, H. 2002: Glacial geology and palaeo-ice dynamics of two ice-sheet margins, Taymyr Peninsula, Siberia and Jameson Land, East Greenland.

49. Sander, M. 2003: Climate signals and frequencies in the Swedish Time Scale, River Ångermanälven, Central Sweden.

50. Zillén, L. 2003: Setting the Holocene clock using varved lake sediments in Sweden.

51. Yu, S.-Y. 2003: The Littorina transgression in southeastern Sweden and its relation to mid-Holocene climate variability.

52. Albrecht, J. 2004: Marginal behaviour of the last Scandinavian Ice Sheet during its final termination and deglaciation over Northeastern Germany.

53. Bergman, J. 2005: Tree-limit ecotonal response to Holocene climatic change in the Scandes Mountains of west-central Sweden.

54. Lindén, M. 2006: Glaciodynamics, deglacial landforms and isostatic uplift during the deglaciation of Norrbotten, Sweden.

55. Jessen, C. A. 2006: The ups and downs of the Holocene: exploring relationships between global CO2 and climate variability in the North Atlantic region.

56. Sparrenbom, C.J. 2006: Constraining the southern part of the Greenland Ice Sheet since the Last Glacial Maximum from relative sea-level changes, cosmogenic dates and glacial-isotatic adjustment models.

57. Kortekaas, M. 2007: Post-glacial history of sea-level and environmental change in the southern Baltic Sea.

58. De Jong, R. 2007: Stormy records from peat bogs in south-west Sweden—implications for regional climatic variability and vegetation changes during the past 6500 years.

59. Schomacker, A. 2007: Dead-ice under different climate conditions: processes, landforms, sediments and melt rates in Iceland and Svalbard.

60. Ljung, K. 2007: Holocene climate and environmental dynamics on the Tristan da Cunha island group, South Atlantic.

61. Håkansson, L. 2008: Glacial history of Northeast Greenland: cosmogenic nuclide constraints on chronology and ice dynamics.

62. Kokfelt, U. 2009: Subarctic ecosystem responses to climate, catchment and permafrost dynamics in the Holocene.

63. Stanton, T. 2011: High temporal resolution reconstructions of Holocene palaeomagnetic directions and intensity: an assessment of geochronology, feature reliability and environmental bias.

64. Nilsson, A. 2011: Assessing Holocene and late Pleistocene geomagnetic dipole field variability.

65. Striberger, J. 2011: Holocene development of Lake Lögurinn and Eyjabakkajökull in eastern Iceland – a multi-proxy approach.

66. Fredh, D. 2012: The impact of past land-use change on floristic diversity in southern Sweden – a quantitative approach based on high-resolution pollen data.

67. Anjar, J. 2012: The Weichselian in southern Sweden and southwestern Baltic Sea: glacial stratigraphy, palaeo- environments and deglaciation chronology.

68. Edvardsson, J. 2013: Holocene climate change and peatland dynamics in southern Sweden based on tree-ring analysis of subfossil wood from peat deposits.

69. Lougheed, B. 2013: Testing palaeomagnetic and 14C based geochronological methods in the Baltic Sea.

70. Randsalu-Wendrup, L. 2013: The palaeolimnological record of regime shifts in lakes in response to climate change.

71. Bragée, P. 2013: A palaeolimnological study of the anthropogenic impact on dissolved organic carbon in South Swedish lakes.

72. Reinholdsson, M. 2014: Magnetic properties of magnetosomal greigite and factors influencing its occurrence and preservation in Baltic Sea Littorina sediments.

73. Mellström, A. 2014: Investigations of temporal changes in climate and the geomagnetic field via high-resolution radiocarbon dating.

74. Åkesson, M. 2014: On the scope of pesticides in ground-water in Skåne, Sweden.

75. Frings, P. 2014: Integrating fluvial processes into the global Si cycle.

76. Adolphi, F. 2014: Solar activity changes at the end of the last ice age—influences on climate and applications for dating.

77. McKay, C. 2015: Benthic environmental responses to climatic changes during the late Quaternary—a micropalaeonto-logical and geochemical approach.

78. Lenz, C. 2015: Manganese cycling in the Baltic Sea over the past ~8000 years—the influence of redox conditions on mineral formation and burial.

79. Alfredsson, H. 2015: Terrestrial Si dynamics in the Arctic—a study on biotic and abiotic controls.

80. Dowling, T.P.F. 2016: The drumlin problem—stream-lined bedforms in southern Sweden.

81. Ning, W. 2016: Tracking environmental changes in the Baltic Sea coastal zone since the mid-Holocene.

82. Fontorbe, G. 2016: Marine silicon cycle through the Cenozoic.

83. Le, T. 2016 : Causal links of past climate change in Coupled Model Intercomparison Project Phase 5 climate models.

84. Bernhardson, M. 2018: Aeolian dunes of central Sweden.

85. Hansson, A. 2018: Submerged landscapes in the Hanö Bay—early Holocene shoreline displacement and human environments in the southern Baltic Basin.

86. Mekhaldi, F. 2018: Cosmogenic radionuclides in environ- mental archives—a paleo-perspective on space climate and a synchronizing tool for climate record.

87. Sigfusdottir, T. 2019: Past dynamics of a marine-terminating glacier in lower Borgarfjörður, west Iceland—analyses of glaciotectonic sediments and landforms.

88. Zheng, M. 2020: Disentangling the production and climate signals from high-resolution Beryllium records: implications for solar and geomagnetic reconstructions.

89. Nantke, C. 2020: Reconstructing Si cycling in transition zones during the Holocene using terrestrial and aquatic records.

90. Yang, B. 2021: Implications of land use on the carbon cycle: Impacts of long-term human activities on terrestrial organic matter input to aquatic ecosystems in southern Sweden.

91. Zahajská, P. 2021: Diatom-rich sediment formation in lakes.

92. Åkesson, S. 2022: Chlorinated aliphatic hydrocarbons: an interdisciplinary study of degradation and distribution in complex environments.

93. Brinkmann, I. 2022: Coastal signals of environmental changes: foraminifera as benthic monitors.

94. Paleari, C. I. 2023: Extreme solar particle storms and links to solar activity inferred from cosmogenic radionuclides in ice cores.

95. Nguyen, H. L. 2023: Solar variability over the Holocene period – disentangling geomagnetic and solar influences on a new continuous 10Be record from Little Dome C, Antarctica.

96. Allington, M. 2023: Improving archaeomagnetic dating through new data acquisition and method development.

97. Benavides Höglund, N. 2024: Improving hydrogeological characterization using groundwater numerical models and multiple lines of evidence.

98. Silvester, E. 2024: Lake ecosystem responses to large volcanic eruptions in recent centuries: diatom and geochemical evidence from varved sediments.

99. Kappelt, N. 2025: Dating Ice Cores with the 36Cl/10Be Ratio.

Printed by Media-Tryck, Lund 2025 NORDIC SWAN ECOLABEL 3041 0903

Quaternary Sciences
Department of Geology
Lund University
Sölvegatan 12
SE-223 62 Lund, Sweden
Telephone +46 46 222 78 80

ISSN 0281-3033
ISBN 9978-91-87847-92-9